Atmos. Meas. Tech. Discuss., https://doi.org/10.5194/amt-2018-21
Manuscript under review for journal Atmos. Meas. Tech.
Discussion started: 13 April 2018

Atmospheric Measurement Techniques Discussions

IASI nitrous oxide (N_2O) retrievals: validation and application to transport studies at daily time scales

Yannick Kangah[1], Philippe Ricaud[1], Jean-Luc Attié[2], Naoko Saitoh[3], Jérôme Vidot[4], Pascal Brunel[4], and Samuel Quesada-Ruiz[1]

[1]CNRM-GAME, Météo-France/CNRS UMR 3589, Toulouse, France
[2]Université de Toulouse, Laboratoire d'Aérologie, CNRS UMR 5560, Toulouse, France
[3]Center for Environmental Remote Sensing, Chiba University, Japan
[4]Centre de Météorologie Spatiale,DP/Météo-France, Lannion, France

Correspondence to: Yannick Kangah (yannick.kangah@umr-cnrm.fr)

Abstract. The aim of this paper is to present a method to retrieve nitrous oxide (N_2O) vertical profiles from the Infrared Atmospheric Sounding Interferometer (IASI) onboard the MetOp platform. We retrieved N_2O profiles using IASI clear sky radiances in 2 spectral bands: B1 and B2 centered at $\sim$1280 cm^{-1} and $\sim$2220 cm^{-1}, respectively. Both retrievals in B1 and B2 (hereafter referred to as N_2O_B1 and N_2O_B2, respectively) are sensitive to the mid-to-upper troposphere with a maximum of sensitivity at around 309 hPa. The degrees of freedom for N_2O_B1 and N_2O_B2 are 1.38 and 0.93, respectively. We validated the retrievals using the High-performance Instrumented Airborne Platform for Environmental Research Pole-to-Pole Observations (HIPPO). The comparisons between HIPPO and the two retrieved datasets show relatively low standard deviation errors around 1.5% ($\sim$4.8 ppbv) and 1.0% ($\sim$3.2 ppbv) for N_2O_B1 and N_2O_B2, respectively. However, the impact of H_2O contamination on N_2O_B1 due to its strong absorption bands in B1 significantly degrades the quality of the retrievals in tropical regions. We analysed the scientific consistency of the retrievals at 309 hPa with a focus on the long-range transport of N_2O especially during the Asian summer monsoon. Over the mid-latitude regions, both variations of N_2O_B1 and N_2O_B2 at 309 hPa are influenced by the stratospheric N_2O-depleted air because of the relative coarse shape of the averaging kernel. The analysis of N_2O_B2 using results from backtrajectories exhibits the capacity of these retrievals to capture long-range transport of air masses from Asia to northern Africa via the summer monsoon anticyclone on a daily basis. Thus, N_2O_B1 and N_2O_B2 offer an unprecedented possibility to study global upper tropospheric N_2O on a daily basis.

1 Introduction

Nitrous oxide (N_2O) is a long-lived greenhouse gas with a lifetime of about 120 years which is essentially produced in the terrestrial and oceanic surfaces by the microbial processes of nitrification and denitrification (Butterbach-Bahl et al., 2013). In terms of radiative forcing, N_2O is the third anthropogenic greenhouse gas after methane (CH_4) and carbon dioxide (CO_2) (Ciais et al., 2014). Its main sink is the photolysis in the stratosphere but it is also destroyed by reacting with the excited atomic oxygen $O(^1D)$. This reaction is the main source of the nitrogen oxides, which are the main responsible of the destruction of the stratospheric ozone. N_2O is therefore becoming the main ozone depleting substance emitted in the 21^{st} century (Ravishankara

Atmos. Meas. Tech. Discuss., https://doi.org/10.5194/amt-2018-21
Manuscript under review for journal Atmos. Meas. Tech.
Discussion started: 13 April 2018

Atmospheric Measurement Techniques Discussions

et al., 2009). The natural and anthropogenic N_2O emissions are about 60% and 40%, respectively (Syakila and Kroeze, 2011; Bouwman et al., 2013). The anthropogenic N_2O emissions are dominated by agricultural sources which represent more than 66% of these emissions. An increase of the N_2O volume mixing ratio (vmr) with a mean rate of 0.75 ppbv.yr^{-1} since the late 1970s has been observed (Ciais et al., 2014). This positive trend is driven by anthropogenic emissions because of the increasing use of nitrogen fertilizers to meet the growing demand of food production, especially in Asia. Moreover, according to the Intergovernment Panel on Climate Change (IPCC), this trend is likely to continue until 2100. Monitoring N_2O emissions and its atmospheric concentration are therefore becoming major issues in the framework of anthropogenic pollution mitigation.

Nowadays, surface measurements of N_2O provide the longer time series of N_2O measurements and are used to characterize the trends and the sources of tropospheric N_2O. Such measurements are performed by several organizations or institutes such as the National Oceanic and Atmospheric Administration/Earth Systems Research Laboratory/Global Monitoring Division (NOAA/ESRL/GMD) or in the framework of joint projects such as the Advanced Global Atmospheric Gases Experiment (AGAGE) (Ganesan et al., 2015) and the Network for the Detection of Atmospheric Composition Change (NDACC) (http://www.ndsc.ncep.noaa.gov). Despite their reliability and the long-term records of surface measurements, their limited geographical coverage makes them difficult to use in order to assess N_2O tropospheric variations at global scale. In addition to surface measurements, there are also some aircraft campaigns like the High-performance Instrumented Airborne Platform for Environmental Research Pole-to-Pole Observations (HIPPO) (Wofsy, 2011; Wofsy et al., 2012) over the Pacific Ocean. N_2O is also measured in some passenger aircraft based measurements including the Comprehensive Observation Network for TRace gases by AIrlLner (CONTRAIL) (Sawa et al., 2015) and the Civil Aircraft for the Regular Investigation of the atmosphere Based on an Instrument Container (CARIBIC) (Assonov et al., 2013).

Since satellite measurements of stratospheric N_2O began in the 1970s, tropospheric N_2O retrievals using satellite measurements are relatively recent. Clerbaux et al. (2009) exhibit the N_2O signature from the infrared measurements of the Infrared Atmospheric Sounding Interferometer (IASI) showing some promising results in view of using these measurements to retrieve N_2O tropospheric profiles. Ricaud et al. (2009a) analysed the equatorial maximum of N_2O during March-May using the operational total columns of N_2O retrieved from IASI measurements using artificial neural networks. These operational N_2O total column products also show seasonal cycles and annual trends consistent with the retrieved N_2O from the ground-based Fourier Transform Spectrometer (FTS) observations at the Izaña Atmospheric Observatory (IZO, Spain) (García et al., 2014, 2016). First results of N_2O total columns retrievals using a partially scanned IASI interferogram with an accuracy of $\pm$13 ppbv ($\sim$4%) are described in Grieco et al. (2013). Retrievals of N_2O tropospheric profiles have been performed using the Atmospheric Infrared Sounder (AIRS) and the results showed interannual trends consistent with surface measurements (Xiong et al., 2014). N_2O profiles retrieved from the Greenhouse Gas Observing Satellite (GOSAT) measurements have been used to study the transport of Asian summertime high N_2O emissions to the Mediterranean upper troposphere (Kangah et al., 2017).

In this paper, we describe the IASI instrument and the Radiative Transfer for Tiros Operational Vertical sounder (RTTOV) used as forward model in our retrieval system in sections 2 and 3, respectively. We present the retrieval strategy and the validation of the results using HIPPO airborne in situ measurements in sections 5 and 6, respectively. In section 7, we analyse the scientific consistency of the retrievals focusing on the long-range transport of N_2O during the Asian summer Monsoon

Atmos. Meas. Tech. Discuss., https://doi.org/10.5194/amt-2018-21
Manuscript under review for journal Atmos. Meas. Tech.
Discussion started: 13 April 2018

Atmospheric Measurement Techniques Discussions

using backtrajectories from the Hybrid Single-Particle Lagrangian Integrated Trajectory model (HYSPLIT) model (Stein et al., 2015). Conclusions are presented in section 8.

2 IASI

IASI is a spaceborne instrument on board the platforms MetOp-A and MetOp-B. The MetOp (Meteorological Operational) mission consists of a series of three sun-synchronous Low Earth Orbits satellites developed jointly by the french space agency (CNES) and the EUropean organization for the exploitation of METeorological SATellites (EUMETSAT). The first satellite (MetOp-A) was launched in October 2006, the second (MetOp-B) in September 2012 and the third (MetOp-C) is expected to be launched in October 2018. MetOp-A and MetOp-B are operational at the present time. The mean MetOp altitude is ∼820 km and the satellite crosses the equator at ∼09:30 mean local solar time and have a repeat cycle of 29 days. MetOp-A and MetOp-B are in the same orbital plane and have an orbit phasing of about 49 min. IASI is a Michelson interferometer that measures infrared spectrum in the spectral range from 645 to 2760 cm^{-1} (15.5 to 3.62 μm) (Clerbaux et al., 2009). Although its apodized spectral resolution is about 0.5 cm^{-1}, IASI provides each spectrum with a sampling of 0.25 cm^{-1} giving a total of 8461 channels. The large spectral domain of IASI contains absorption bands of several atmospheric constituents (Hilton et al., 2012) among which the major absorbers are water vapour (H_2O), ozone (O_3), CO_2, N_2O, CH_4 and carbone monoxide (CO). IASI observes the Earth with a swath of about 2200 km (1100 km on each side) and its instantaneous field of view is composed of four circular pixels of 12 km diameter footprint on the ground at nadir. The operational IASI H_2O, temperature and O_3 products are retrieved simultaneously using an optimal estimation method (Pougatchev et al., 2009; Rodgers et al., 2000) whereas total columns of the other molecules are retrieved using artificial neural networks (Turquety et al., 2004). In this work, we used the IASI level 1c spectra (calibrated and apodized spectra) to perform our retrievals.

3 RTTOV

RTTOV is a fast model of transmittances of the atmospheric gases that are generated from a database of accurate line-by-line (LBL) transmittances (Saunders et al., 1999). The database of accurate transmittances is generated from a set of diverse atmospheric profiles and then a linear regression is computed linking the optical depths of the vertical layers and a set of atmospheric profile-dependent predictors. The regression coefficients are actually given for different Instrument Spectral Response Functions (ISRF) including the ones of IASI. For our retrieval system, we used RTTOV version 11.2 together with the regression coefficients v9 based on the model LBLRTM (LBL Radiative Transfer Model) (Hocking et al., 2015). In this version, the predictors depend on the trace gases profiles including H_2O, O_3, CO_2, N_2O, CH_4 and CO. It takes less than 25 ms to compute 183 IASI channels together with weighting functions using an input of atmospheric profiles on 54 vertical levels and surface emissivities. Comparing with accurate LBL models, the biases of RTTOV simulations for IASI Brightness Temperature (BT) over sea in clear sky conditions are within ±1 K in the spectral range 645 to 2000 cm^{-1} and within ±1.6 K in the N_2O/CO_2 $\nu 3$ region between 2200 and 2300 cm^{-1} (Matricardi, 2009).

Atmos. Meas. Tech. Discuss., https://doi.org/10.5194/amt-2018-21
Manuscript under review for journal Atmos. Meas. Tech.
Discussion started: 13 April 2018

Atmospheric Measurement Techniques Discussions

4 N_2O absorption bands

Previous studies from Clerbaux et al. (2009) have highlighted three absorption bands of N_2O in the IASI spectral range centered at ∼1280 cm^{-1}, ∼2220 cm^{-1} and ∼2550 cm^{-1}. Figure 1 shows a N_2O weighting function matrix (called hereafter Jacobian matrix) calculated in units of brightness temperature (BT) using a N_2O profile derived from the Michelson Interferometer for Passive Atmospheric Sounding (MIPAS) reference atmosphere (V3) daytime mid-latitude climatology. This matrix represents the sensitivity of the calculated BT to a unit change in the N_2O volume mixing ratio (vmr). The spectral signature of N_2O appears in the three spectral regions with significant differences of intensity. The most intense absorption band (called hereafter B2) is between 2190 and 2240 cm^{-1} and shows sensitivity to N_2O from the lowermost troposphere to 100 hPa with a maximum of sensitivity between 500 and 200 hPa. The absorption band located between 1250 and 1310 cm^{-1} (called hereafter B1) is less intense than B2 and is sensitive to N_2O between 800 and 100 hPa. The third band (called hereafter B3) located between 2500 and 2600 cm^{-1} is much less intense than B1 and B2 and is sensitive to N_2O from 900 to 300 hPa. To illustrate the sensitivity of these three bands to N_2O and to the other atmospheric and surface parameters, a sensitivity study has been performed using the MIPAS climatology for N_2O, CO_2 and O_3 profiles and a set of atmospheric and surface parameters representative of a given atmospheric state on 13 June 2011 at 11.8°N and 142.9°W. This study consists in calculating of the variation of the BT (called hereafter ΔBT) over the IASI spectral range for a given variation of the major atmospheric and surface parameters consistent with their actual accuracy. Figure 2 shows the absolute value of the ΔBT ($|\Delta BT|$) for variations of each major absorber (H_2O, O_3, CO_2, N_2O, CH_4 and CO) and for variations of temperature and surface temperature. The IASI radiometric noise expressed as the Noise Equivalent Delta Temperature (NEDT) is superimposed to the $|\Delta BT|$ signals. In each band, channels were selected by optimizing the Signal to Noise Ratio (SNR) while reducing the spectral signature of the other parameters. B1 is mainly impacted by temperature, H_2O, CH_4 and surface temperature. The signal corresponding to 10% change of H_2O is more than twice greater than the signal corresponding to a change of N_2O by 4% in most spectral domains of B1. The signal corresponding to a change of CH_4 by 2% is half the size to the signal of N_2O. A total of 126 channels is selected in B1. The signal of N_2O is twice larger than the NEDT for all selected channels in B1 whilst CH_4, H_2O and temperature are critical parameters for the N_2O retrieval using the 126 selected channels in B1. In B2, we selected a total of 103 channels where the signal of N_2O is more than twice greater than the signals of the other parameters except for atmospheric temperature and NEDT. The NEDT level of magnitude is similar to the signal of N_2O while the $|\Delta BT|$ signal corresponding to the temperature variation is slightly greater than that of N_2O. The radiometric noise and the atmospheric temperature are therefore the critical parameters for the N_2O retrieval in B2. In B3, we selected no channels because the radiometric noise is too large compared to the signal of N_2O. In summary, the absorption band of N_2O in B2 is sufficiently isolated from the absorption band of the other gases but presents the same level of magnitude as the IASI radiometric noise whereas in B1 the signal of N_2O is more than twice greater than the noise but is impacted by the absorption bands of CH_4 and H_2O.

Atmos. Meas. Tech. Discuss., https://doi.org/10.5194/amt-2018-21
Manuscript under review for journal Atmos. Meas. Tech.
Discussion started: 13 April 2018

Atmospheric Measurement Techniques Discussions

5 Retrieval Strategy

5.1 Methodology

We used an optimal estimation method based on the Levenberg-Marquardt iterative algorithm (Rodgers et al., 2000) to retrieve N_2O profiles over 13 fixed pressure levels from IASI clear sky radiances in the bands B1 and B2. Hereafter, the retrievals in B1 and B2 are referred to N_2O_B1 and N_2O_B2, respectively. In the retrieval algorithm, the i+1th retrieval vector is expressed as:

$$\hat{X}_{i+1} = X_a + (K_i^T S_y^{-1} K_i + \gamma S_a^{-1})^{-1} \times \{K_i^T S_y^{-1}([Y - F(\hat{X}_i)] + K_i[\hat{X}_i - X_a]) + \gamma S_a^{-1}[\hat{X}_i - X_a]\} \quad (1)$$

where X_a is an a priori vector with an error covariance matrix S_a. Y is the observed radiances with an error covariance matrix S_y. $F(\hat{X}_i)$ and K_i are the calculated forward spectrum and the Jacobian matrix at the iteration i, respectively. γ is the Levenberg-Marquardt parameter (Rodgers et al., 2000). The vertical sensitivity of the retrieval can be characterised using the averaging kernel matrix (A) defined as:

$$A = \frac{\partial \hat{X}}{\partial X} = (K^T S_y^{-1} K + S_a^{-1})^{-1} K^T S_y^{-1} K \quad (2)$$

N_2O_B1 profiles are retrieved simultaneously with the vmr profiles of H_2O and CH_4 whilst N_2O_B2 profiles are retrieved simultaneously with the vmr profiles of H_2O, CO and CO_2. The air temperature profiles and the surface parameters (temperature and emissivity) are also retrieved simultaneously with the N_2O profiles for N_2O_B1 and N_2O_B2.

The a priori error covariance matrix S_a is calculated as follows:

$$Sa_{ij} = \sigma_a^2 \times exp(-|ln(P_i) - ln(P_j)|) \quad (3)$$

where σ_a^2 is an a priori variance error fixed for each parameter of the state vector and P_i the pressure level at the level i.

For the retrievals, we used a fixed N_2O a priori profile derived from the MIPAS V3 reference atmosphere daytime mid-latitude climatology. Since this climatology is given for the year 2001, we adjusted it for the year 2011 by applying the averaged increase rate of 0.75 ppbv.yr^{-1} consistently with Ricaud et al. (2009b). We fixed σ_a for the N_2O profile to 4% consistently with Grieco et al. (2013).

The a priori states of H_2O, temperature and surface temperature were taken from the IASI level 2 operational products (August et al., 2012). A validation using radiosonde data gave a standard error (std) of $\sim$2 K for the surface temperature, of about 10% for the relative humidity and between 0.6 and 1.5 K for the temperature profile (Pougatchev et al., 2009). Thus, we took for N_2O_B1 and N_2O_B2, σ_a values of 1 K and 2 K for the temperature profile and the surface temperature, respectively. A σ_a value of 10% for the H_2O profile was used for N_2O_B2. Clerbaux et al. (2009) show the presence of a relatively strong absorption band of the deuterium hydrogen oxide (HDO) also called semiheavy water in the band B1. However, this chemical

Atmos. Meas. Tech. Discuss., https://doi.org/10.5194/amt-2018-21
Manuscript under review for journal Atmos. Meas. Tech.
Discussion started: 13 April 2018

Atmospheric Measurement Techniques Discussions

species is not taken into account as a variable parameter in RTTOV. Therefore, after sensitivity studies, we fixed the σ_a value for the H_2O profile to 30% for N_2O_B1. In a similar approach to the N_2O a priori profile, we took the CO_2 a priori from the MIPAS reference atmosphere v3 daytime mid-latitude climatology and applied an annual trend of 2.3 ppmv.yr^{-1} (Ciais et al., 2014). A σ_a of 2% is used for the CO_2 a priori profile after a sensitivity study.

In addition, CH_4 and CO a priori profiles were taken from the Monitoring Atmospheric Composition and Climate (MACC) project reanalysis (Inness et al., 2013). σ_a was fixed to 10% for CO after a sensitivity study and consistently with the CO validation reports (http://www.gmes-atmosphere.eu/services/aqac/global_verification/validation_reports/). For CH_4, σ_a was fixed to 2% which is approximately the std error on the IASI retrieved CH_4 profiles (Xiong et al., 2013). The land surface a priori emissivity is derived from a global atlas of land surface emissivity based on inputs from the Moderate Resolution Imaging Spectroradiometer (MODIS) operational product (Borbas and Ruston, 2010; Seemann et al., 2008). Over sea surface, we used the version 6 of the Infrared Surface Emissivity Model (ISEM) (Sherlock and Saunders, 1999) as an a priori surface emissivity. σ_a is fixed to 10% for the surface emissivity since this parameter is also used as a sink parameter. An observation error diagonal covariance matrix S_y was used for the retrievals in both bands with the IASI radiometric noise as the diagonal elements of the matrix.

5.2 Data quality control

To assess the quality of the retrieved N_2O profiles, we used quality parameters derived from the optimal estimation theory (Rodgers et al., 2000). Our retrieval process consists in the minimization of the cost function χ^2 defined as:

$$\chi^2 = \frac{([\hat{X} - X_a]^T S_a^{-1}[\hat{X} - X_a]) + ([Y - F(\hat{X})]^T S_y^{-1}[Y - F(\hat{X})]}{dim(\hat{X}) + dim(Y)} \quad (4)$$

where $dim(\hat{X})$ and $dim(Y)$ are the dimensions of the state vector and of the radiances (number of channels), respectively. χ^2 allows to evaluate the quality of the retrieval by combining the calculated residuals relative to the observations error covariance matrix and the difference between the estimated and the a priori profiles relative to the a priori error covariance matrix. In our case, we performed simultaneous retrievals for both N_2O_B1 and N_2O_B2. Therefore, the χ^2 derived from the optimal estimation theory is a quality control parameter for the whole retrieved state vectors which include N_2O profiles and the other interfering parameters. In addition to χ^2, we computed another variable to assess the quality of the retrieved tropospheric N_2O profile which is our target species. Thus, we calculate the difference between the a priori and the retrieved N_2O relative to the N_2O a priori errors σ_a. This variable called $\chi^2_{N_2O}$ is defined as:

$$\chi^2_{N_2O} = \frac{\sum_{P_j<1000\ hPa}^{P_j>200\ hPa} [\hat{X}_j - X_{a_j}]^2 \beta_{a_j}}{n_p} \quad (5)$$

where $\hat{X}_j$ and X_{a_j} are the retrieved and the a priori N_2O at the pressure level P_j, respectively. β_{a_j} is the diagonal element of the a priori error precision matrix (the inverse of the a priori error covariance matrix) at the pressure level P_j and n_p is the

Atmos. Meas. Tech. Discuss., https://doi.org/10.5194/amt-2018-21
Manuscript under review for journal Atmos. Meas. Tech.
Discussion started: 13 April 2018

Atmospheric Measurement Techniques Discussions

number of levels used for the calculation.

An upper limit for the χ^2 parameter is generally used to select good quality pixels. For instance, an upper limit of 3 on a χ^2 calculated in the radiances space was used to select good quality pixels for CH_4 retrievals from IASI measurements (Xiong et al., 2013). Following the same methodology, we applied an upper limit on $\chi^2_{N_2O}$ to select good quality pixels. After performing sensitivity studies for both N_2O_B1 and N_2O_B2, we rejected all the data with a χ^2 or a $\chi^2_{N_2O}$ greater than or equal to 4.

Moreover, to evaluate the impact of the other retrieved parameters on N_2O_B1 and N_2O_B2, we calculated the Contamination Factor (called hereafter CF) defined as follows:

$$CF(i) = \sum_j \left| \frac{\partial \hat{x}_i}{\partial c_j} \right| \frac{\Delta c_j}{\hat{x}_i} \times 100 \tag{6}$$

Here, $CF(i)$ is the contamination of the parameter c on the retrieved N_2O at the level i ($\hat{x}_i$). Δc_j is the uncertainty on the parameter c at the level j. We fixed Δc_j to the a priori error σ_a for each parameter. Then for the parameter c, we defined $CF_{tot}(c)$ as the sum of the CF over the 13 retrieval levels. CF indicates the influence of the uncertainties in the knowledge of the co-retrieved parameters on the variability of the target species N_2O retrievals. Here, the uncertainties on the co-retrieved parameters have been fixed to the a priori uncertainties. Thus, CF does not take into account the effects due to the spatial and temporal variations of these uncertainties. But CF estimates, a priori, how critical is the characterisation of each co-retrieved parameter for the quality of the N_2O retrievals. As consequence, a posteriori sensitivity studies should be performed on each critical parameter to determine which co-retrieved parameters uncertainties have the most significant impact on the quality of the N_2O retrievals.

6 Validation

In this section, we analyse the performance of our retrieval system by comparing the results with the in-situ measurements from the five HIPPO airborne campaigns (Figure 3): HIPPO 1 (January 2009), HIPPO 2 (October-November 2009), HIPPO 3 (March-April 2010), HIPPO 4 (June-July 2011) and HIPPO 5 (August-September 2011). For this purpose, we processed 26850 N_2O_B1 and N_2O_B2 profiles along the flight paths from the five HIPPO campaigns. Using a similar method as explained in Kangah et al. (2017), we used for these comparisons the measurements from the Harvard/Aerodyne Quantum Cascade Laser Spectrometer (QCLS), one of the airborne instruments of HIPPO, and the retrieved profiles selected within a collocation temporal and spatial window of $\pm$200 km and $\pm$12h, respectively. Our aim is to characterise the retrieval errors as well as the ability of the retrieval system to capture N_2O tropospheric variations.

6.1 Error Characterisation

The total retrieval errors can be divided into four components: a smoothing error, a forward model error, a model parameter error and a retrieval noise. We used a simultaneous retrieval strategy to include all the parameters which influence RTTOV in

Atmos. Meas. Tech. Discuss., https://doi.org/10.5194/amt-2018-21
Manuscript under review for journal Atmos. Meas. Tech.
Discussion started: 13 April 2018

Atmospheric Measurement Techniques Discussions

each band and we removed RTTOV systematic biases consistently with Matricardi (2009). Therefore, the forward model and the model parameter errors can be, as a first approximation, considered as negligible compared to the smoothing error and the retrieval noise. The covariance matrix of the smoothing error (S_s) is defined as:

$$S_s = (A - I)S_e(A - I)^T \tag{7}$$

where A is the N_2O averaging kernels matrix; I is the identity matrix and S_e is the covariance matrix of the real ensemble of states consistently with Rodgers et al. (2000). For our retrieval algorithm, we use a simple "ad hoc" matrix (see Eq. 3) as a priori covariance matrix (S_a) to constrain the retrieval system. Since this matrix may or may not be representative of the variability of a real ensemble of N_2O profiles, we took S_e as the covariance matrix of HIPPO profiles.
The retrieval noise covariance matrix (S_n) is defined as:

$$S_n = GS_yG^T \tag{8}$$

where G is the gain matrix which represents the change in the vmr profile for a unit change in the observation Y. The theoretical covariance matrix of the total errors (S_{tot}) is therefore defined as:

$$S_{tot} = S_s + S_n \tag{9}$$

The theoretical covariance matrix of the total errors is then compared with an empirical total errors covariance matrix calculated using the HIPPO measurements and the retrievals along the HIPPO campaigns flight paths (namely the covariance matrix of the difference between HIPPO profiles and IASI retrieved profiles). Figure 4 shows the standard deviation errors (std errors) corresponding to all these covariance matrices (square roots of the diagonal elements of the covariance matrix) and averaged over the set of retrievals for N_2O_B1 and N_2O_B2. The empirical std error which we consider as our reference standard deviation of the total errors (σ_{tot}) is about 1.5% (∼4.8 ppbv) for N_2O_B1 and about 1.0% (∼3.2 ppbv) for N_2O_B2 in the troposphere. For N_2O_B2, the theoretical σ_{tot} is consistent with the empirical σ_{tot} but, for N_2O_B1, the theoretical σ_{tot} is about 0.5% less than the empirical σ_{tot}. This means that our hypothesis of two sources of errors to characterise the total error is correct for N_2O_B2 but is not enough for N_2O_B1 for which other sources of error should be considered (forward model errors and/or model parameter errors). Concerning the forward model errors, we removed the biases on RTTOV IASI clear sky radiances consistently with Matricardi (2009) both in the band B1 and B2. Therefore the difference between the theoretical and the empirical std errors for N_2O_B1 is certainly due to the existence of other sources of variation of the radiances in the band B1 which are not correctly taken into account in our retrieval system. The HDO absorption which is the only significant absorption band not included in the predictor parameters of RTTOV could be responsible of at least part of these unexplained variations. To summarise, we can consider that the std errors on N_2O_B1 and N_2O_B2 are on averaged about 1.5% (∼4.8 ppbv) and 1.0% (∼3.2 ppbv), respectively. However, for the users, the retrieved profiles will be given with the empirical S_{tot} together with the theoretical S_{tot} associated with each retrieval.

Atmos. Meas. Tech. Discuss., https://doi.org/10.5194/amt-2018-21
Manuscript under review for journal Atmos. Meas. Tech.
Discussion started: 13 April 2018

6.2 Sensitivity in the observation and retrieval spaces

Figure 5 shows the averaged observed and calculated (using a priori and retrievals) radiances together with the averaged calculated residuals for both B1 and B2. In B1, the mean residual is reduced from -0.8% (using the a priori) to 0.01% (using the retrievals) whereas in B2, the mean residual is reduced from -0.5% (using the a priori) to 0.01% (using the retrievals). The differences between the a priori residuals in B1 and B2 are due to the existence of more interfering parameters in B1 than in B2. Therefore, some differences between N_2O_B1 and N_2O_B2 due to the contamination of CH_4 and H_2O are expected. Figures 6 and 7 show the mean N_2O normalized (Deeter et al., 2007) averaging kernels matrix together with the altitude of the kernels maximum and the mean CF from CH_4, temperature, surface temperature and H_2O for N_2O_B1 and N_2O_B2, respectively. Considering the averaging kernels, the maximum of sensitivity is located at the retrieval level 309 hPa for both N_2O_B1 and N_2O_B2. In addition, the averaging kernels corresponding to this level peak at 309 hPa. Therefore, retrieved vmrs at this level are the most reliable for both N_2O_B1 and N_2O_B2. For N_2O_B2, all the averaging kernels peak at the levels 309 hPa. This means that the retrieved N_2O vmr profiles are mainly sensitive to the real N_2O vmr at this level. This result is consistent with previous studies from Kangah et al. (2017) and Xiong et al. (2014). The degree of freedom (DOF), which represents the number of independent vertical pieces of information of the retrieved profile and is computed as the trace of the averaging kernels matrix, is on average equal to 1.38 and 0.93 for N_2O_B1 and N_2O_B2, respectively. The DOF for N_2O_B1 is greater than that of N_2O_B2 because the SNR is higher in B1 than in B2. Thus, more channels with better SNR are selected in B1 than in B2. Although the retrieved N_2O is impacted by temperature in the two bands, we have in B1 an additional significant impact of CH_4 and H_2O. In conclusion, we expect more contamination on N_2O_B1 than on N_2O_B2.

6.3 Retrieval accuracy

To assess the skills of the retrieval process, we applied the IASI N_2O averaging kernels to the HIPPO profiles using the following equation (Rodgers et al., 2000):

$$\hat{x} = Ax + (I - A)x_a \tag{10}$$

where x_a is the IASI a priori profile, x the HIPPO profile, $\hat{x}$ the result of the averaging kernels application (called hereafter convolved HIPPO), I the identity matrix and A the IASI N_2O averaging kernels matrix.

Figures 8 and 9 show the results from the comparisons between HIPPO measurements and N_2O_B1 and N_2O_B2 averaged within the spatial and temporal window around the HIPPO measurements, respectively. N_2O_B1 and HIPPO measurements are moderately correlated (the Pearson linear correlation coefficient R=0.42) with a low bias and standard deviation (called hereafter std) error of -1.6 ppbv (∼0.5%) and 3.5 ppbv (∼1.0%), respectively. However, the quality of the retrievals depends on the latitude band. The consistency between N_2O_B1 and HIPPO increases at mid-latitudes (e.g. R=0.63 for northern hemisphere mid-latitudes). We can also notice that there is a very low mean bias (-0.1 ppbv) in the northern hemisphere high-latitude regions.

Atmos. Meas. Tech. Discuss., https://doi.org/10.5194/amt-2018-21
Manuscript under review for journal Atmos. Meas. Tech.
Discussion started: 13 April 2018

Atmospheric Measurement Techniques Discussions

Furthermore, N_2O_B1 exhibits greater biases in tropical regions (-3.7 and -4.8 ppbv in the tropical northern and southern hemispheres, respectively) than in the other regions. Figure 6 suggest that the largest CF on N_2O_B1 are from the temperature, CH_4 and H_2O, respectively. To understand the degradation in the quality of N_2O_B1 over the tropics, we examined the contamination of H_2O, CH_4 and temperature (see Eq. 6). For that purpose, we filtered N_2O_B1 over the northern hemisphere tropical regions by considering the pixels with $CF_{tot}(H_2O)$, $CF_{tot}(CH_4)$ and CF_{tot}(temperature) less than arbitrary maxima called $CF_{tot}^{max}(H_2O)$, $CF_{tot}^{max}(CH_4)$ and CF_{tot}^{max}(temperature), respectively. Then, we evaluated the mean bias (N_2O_B1 − HIPPO) using these filtered N_2O_B1. In order to have enough collocated IASI-HIPPO pixels, N_2O_B1 around the HIPPO measurements are not averaged for this sensitivity study (see Figure 10). We observe that the lower $CF_{tot}^{max}(H_2O)$, the better the bias, whereas there is no significant improvement of the bias when we used $CF_{tot}^{max}(CH_4)$ and CF_{tot}^{max}(temperature) to filter N_2O_B1. Thus, when $CF_{tot}^{max}(H_2O)$ decreases from 10 to 4, the absolute value of the mean bias decreases from 2.5 to 1.0 ppbv. Therefore, we can consider that the degradation of the quality of N_2O_B1 over the tropics is mainly due to the contamination of H_2O. Although CF_{tot}(temperature) and $CF_{tot}(CH_4)$ are greater than $CF_{tot}(H_2O)$, H_2O is actually the most critical parameter in the band B1 to retrieve N_2O in our retrieval system. H_2O has a high variability, especially over the tropical regions where maxima of H_2O vmrs are observed. This variability is more difficult to retrieve than the variability of temperature and CH_4. Thus, August et al. (2012) show that the std error on the IASI retrieved temperature at 800 hPa varies from 1 K (northern hemisphere sea) to 1.5 K (tropical land) whereas the std error on the IASI retrieved H_2O at 800 hPa varies from 1500 ppmv (northern hemisphere sea) to 3500 ppmv (tropical land). Furthermore, we evaluated the linear correlation R and the std error using the different values of $CF_{tot}^{max}(H_2O)$ (see Figure 11). When $CF_{tot}^{max}(H_2O)$ decreases from 10 to 4, R increases from 0.17 to 0.57 and the std error decreases from 3.5 to 3.0 ppbv. $CF_{tot}(H_2O)$ should therefore be considered carefully when analysing N_2O_B1 over tropical regions.

N_2O_B2 is moderately correlated with HIPPO measurements (R=0.6) with a std error of 3.2 ppbv and a very low mean bias of 0.3 ppbv. This moderate correlation is also observed when considering only data from the northern hemisphere mid-latitudes. In the northern hemisphere tropical regions, the bias is slightly higher (-1.0 ppbv) and the correlation coefficient decreases to 0.31. The worst correlation coefficient is found for the southern hemisphere mid-latitudes (R=0.11). The very small slope ($\sim$0.16) indicates that N_2O_B2 does not capture optimally the N_2O spatial and temporal variations in this region, although we observe a relatively low mean bias (1.6 ppbv) in this region. In tropical regions the correlation coefficient between N_2O_B2 and HIPPO measurements becomes very high (0.71 and 0.92 in the northern and southern hemispheres, respectively) compared to the other regions. However, the large slope from the linear regression (2.51 and 3.32 in the northern and southern hemispheres, respectively) indicates that N_2O_B2 tends to overestimate the spatial and temporal N_2O vmr gradients in this region.

In summary, N_2O_B1 and N_2O_B2 are of sufficient quality to be used to analyse N_2O variations in the mid and high latitude regions. N_2O_B2 can even be used to analyse N_2O transport processes between tropical regions and higher latitude regions whereas, for N_2O_B1, we have to analyse vmrs in the tropics taking care to reject retrievals with high $CF_{tot}(H_2O)$. The scientific users should fix $CF_{tot}^{max}(H_2O)$ to filter N_2O_B1 according to their need in terms of accuracy and/or spatial and temporal sampling. The statistics presented on Figure 11 can be used for that purpose.

Atmos. Meas. Tech. Discuss., https://doi.org/10.5194/amt-2018-21
Manuscript under review for journal Atmos. Meas. Tech.
Discussion started: 13 April 2018

Atmospheric Measurement Techniques Discussions

7 Tropospheric variations of N_2O_B1 and N_2O_B2 related to long-range transport

Since we averaged IASI retrievals over a temporal and spatial window of ±200 km and ±12h for the validation at 309 hPa (see Section 6.3), for the following analyses, our basic pixel for both N_2O_B1 and N_2O_B2 is a daily mean within a 4° × 4° horizontal grid. Figure 12 shows maps of N_2O_B1, $CF_{tot}(H_2O)$ and N_2O_B1 filtered with $CF_{tot}^{max}(H_2O)$ equal to 4 at 309 hPa and averaged over 3 days (27-29 July 2011). The horizontal winds from the ERA-Interim reanalysis are superimposed on the N_2O_B1 maps. Figure 13 shows maps of N_2O_B2 superimposed with horizontal winds from the ERA-Interim reanalysis at 309 hPa and averaged over 4 periods of 3 days: 21-23 July, 24-26 July, 27-29 July and 30 July-01 August 2011. The maps of tropopause pressure averaged over the same 4 periods are presented on Figure 14. The horizontal distribution of N_2O_B1 at 309 hPa over the period 27-29 July 2011 (Figure 12 top) shows:

1. strong maxima (≥330 ppbv) within a band elongated from the Sahara to minor Asia and Iran with a maximum located over the North-Eastern China and

2. strong minima over Europe, the Atlantic Ocean and the Mongolian plateau with some localized minima in the equatorial/tropical band (Arabian Sea, Indian Ocean, South China Sea).

$CF_{tot}(H_2O)$ associated to N_2O_B1 over the same period (Figure 12 center) is, on average, less than 5 in the mid-latitudes but greater than 6 in the tropics, underlining the great impact of the high H_2O contamination on N_2O_B1 in the tropical band. When filtering N_2O_B1 with $CF_{tot}^{max}(H_2O)$ equal to 4, only the N_2O_B1 retrieved in the mid-latitudes is maintained (Figure 12 bottom). The so filtered N_2O_B1 shows a longitudinal distribution in the mid-latitudes. According to wind patterns, the maxima of N_2O_B1 centered around 50°E and 70°E in longitude are influenced by the N_2O-enriched air originated from the tropics whilst the minima of N_2O_B1 between 10°W and 10°E in longitude are influenced by the N_2O-depleted air originated from high latitudes.

Consistently with previous studies from Ricaud et al. (2009a) and Kort et al. (2011), the horizontal distribution of N_2O_B2 (Figure 13) over the 4 periods shows maxima (≥330 ppbv) in the tropics and minima (≤325 ppbv) in the mid-latitudes. Moreover, there are local maxima and minima of N_2O_B2 in the mid-latitudes consistent with, on the one hand, the wind patterns and, on the other hand, the variations of the tropopause pressure level (Figure 14). Thus, the minimum of N_2O_B2 in the mid-latitudes are due, on the one hand, to the influence of N_2O-depleted air from the stratosphere and on the other hand to the influence of air-masses originated from the high latitudes. Previous studies from García et al. (2014, 2016) also highlighted this influence of stratospheric air masses on the seasonality of the IASI operational retrievals of N_2O total columns at Izaña (Spain). The tropopause pressure levels displayed on Figure 14 show two maxima between 40°N and 50°N and within longitude bands (10°W-30°E and 80°E) consistent with the N_2O_B2 minima. The influence of stratospheric N_2O on N_2O_B2 (and also on N_2O_B1 as shown in Figure 12) is due to the width of the averaging kernel at 309 hPa with a half-maximum from ∼600 to ∼100 hPa. Kangah et al. (2017) show a connection between the high N_2O surface emissions over Asia in summer and the upper tropospheric N_2O patterns over the Mediterranean basin. Actually, high N_2O surface emissions related to high soil water content occur over Asia (especially eastern China and the Indian/Tibetan plateau region) and are transported in the upper

Atmos. Meas. Tech. Discuss., https://doi.org/10.5194/amt-2018-21
Manuscript under review for journal Atmos. Meas. Tech.
Discussion started: 13 April 2018

troposphere and redistributed westward by the easterly winds associated to the Asian summer monsoon anticyclone. Wind patterns on Figure 12 show the connection between the western Asia region and the eastern Mediterranean region. Thus, long-range transport processes between Asia and the eastern Mediterranean are expected. A maximum of N_2O_B1 (∼331 ppbv) is also observed over the eastern Mediterranean as a result of these transport processes. N_2O_B1 also exhibits maxima over the eastern China (∼332 ppbv) which is the result of the vertical transport to the upper troposphere of the high summertime N_2O emissions over this region. The high emissions and vertical transport are confirmed by the occurrence of relatively high convective precipitations over the eastern China region the days before (24-26 July, not shown).

To highlight these long-range transport processes, we used the HYSPLIT model (Stein et al., 2015) to perform a 4-day back-trajectory ensemble from a central point located in the upper troposphere (∼306 hPa) of the northern Africa (25°N, 32°E) on 28 July 2011 at 12h00 UTC. Then, N_2O_B2 along the path of the air masses represented by the mean trajectory is evaluated. Figure 15 shows the results of the backtrajectories with air masses transported from western Asia to northern Africa. Furthermore, the mean trajectory is located on a vertical range 420-316 hPa which is in the domain of vertical sensitivity of N_2O_B2 considering the shape of the averaging kernel for the level 309 hPa (Figure 7). To study N_2O_B2 along the mean trajectory, we calculated a Hovmöller diagram using the latitudinal range of the backtrajectory ensemble from 21 to 31°N. This diagram calculated on a daily basis for the longitude range from 30 to 80°E and superimposed with zonal winds from the ERA-Interim reanalysis is presented in Figure 16. As expected, the mean daily trajectory represented by the black stars is located in an easterly wind region (delimited by the blue contours). Moreover, this diagram exhibits the transport of high N_2O_B2 maximum by the easterly wind fluxes associated to the Asian monsoon anticyclone. N_2O_B2 corresponding to the mean trajectory and averaged over the latitude range of the Hovmöller diagram are within the range 330.5-331.5 ppbv. We averaged a maximum of 3 basic ($4^\circ \times 4^\circ$) pixels over the latitude range of the Hovmöller diagram. Since the std error for a single N_2O_B2 pixel is about 2.8 ppbv (see Section 6.3), we can approximate the error on the retrieved N_2O_B2 over the mean trajectory by $2.8/\sqrt{3} \approx$ 1.6 ppbv. Therefore, we can conclude that N_2O_B2 allows to follow the upper tropospheric N_2O transport processes between tropical and mid-latitude regions at nearly daily time scales.

8 Conclusions

We presented and validated an inversion algorithm to retrieve N_2O profiles using IASI level 1c radiances. Consistently with previous studies, the N_2O Jacobian exhibits three N_2O absorption bands: B1 centered at ∼1280 cm^{-1}, B2 centered at ∼2220 cm^{-1} and B3 centered at ∼2550 cm^{-1}. We performed a sensitivity test in each band studying the radiometric noises and the signals from N_2O, temperature, surface temperature and other major absorbers including CH_4, H_2O, CO, O_3, CO_2. By maximizing the SNR and minimizing the impact from the interfering parameters in each bands, 126 channels in B1 and 103 channels in B2 were selected to retrieve N_2O profiles. We also deduced from this sensitivity study that, in addition to the impact of temperature and surface temperature, B1 is impacted by relatively strong absorption bands of CH_4 and H_2O whereas B2 has relatively strong radiometric noises. A retrieval algorithm based on the Levenberg-Marquardt optimal estimation theory was used to retrieve N_2O profiles using B1 and B2 (namely N_2O_B1 and N_2O_B2, respectively). N_2O_B1 was retrieved simultane-

ously with CH_4, H_2O, temperature, surface temperature and surface emissivity whereas N_2O_B2 was retrieved simultaneously with H_2O, temperature, CO, CO_2, surface temperature and surface emissivity. Consistently with the previous studies (Xiong et al., 2014; Kangah et al., 2017), both N_2O_B1 and N_2O_B2 are sensitive to mid-to-upper troposphere with a maximum of sensitivity in the upper troposphere ($\sim$309 hPa).

We developed quality control parameters based on the standard χ^2 derived from the optimal estimation theory and on a reduced χ^2 parameter called $\chi^2_{N_2O}$. χ^2 gives a quality criteria for the whole state vector and $\chi^2_{N_2O}$ gives a quality criteria for the N_2O tropospheric profile. Besides these two parameters, another quality control parameter based on $CF_{tot}(H_2O)$ was used to assess the impact of the H_2O contamination on N_2O_B1, especially in tropical regions. N_2O_B1 and N_2O_B2 at 309 hPa are validated using HIPPO airborne in situ measurements. From these comparisons, we calculated std errors around 1.5% and 1.0% for N_2O_B1 and N_2O_B2, respectively. Besides, we calculated relatively low biases (-1.6 ppbv for N_2O_B1 and 0.3 ppbv for N_2O_B2). Apart from an overestimation of gradients in tropical regions, N_2O_B2 is of a good quality in all latitudinal bands. The quality of N_2O_B1 is good except in tropical regions where H_2O contamination characterised by high $CF_{tot}(H_2O)$ degraded the quality of the retrievals.

We studied the scientific consistency of the retrieved N_2O by focusing on transport processes. We showed that both N_2O_B1 and N_2O_B2 variations over the mid-latitudes regions are influenced by the N_2O-depleted air from high latitudes and from the stratosphere. Using backtrajectory calculations, we also showed that the transport of high Asian N_2O emissions from Asia to the Eastern Mediterranean basin by the summertime Asian monsoon anticyclone can be observed using N_2O_B2 on a daily basis. N_2O_B1 also offers good opportunities to study this N_2O transport process but with limitations due to H_2O contamination over the tropics. Thus, at this stage of our retrieval process, N_2O retrieved in bands B1 and B2 offer an unprecedented possibility to study upper tropospheric N_2O on a daily basis at global scale. This algorithm will be therefore applied to retrieve N_2O profiles at a global scale using the 10 years of IASI measurements.

References

Assonov, S., Brenninkmeijer, C., Schuck, T., and Umezawa, T.: N2O as a tracer of mixing stratospheric and tropospheric air based on CARIBIC data with applications for CO2, Atmospheric environment, 79, 769–779, https://doi.org/10.1016/j.atmosenv.2013.07.035, 2013.

August, T., Klaes, D., Schlüssel, P., Hultberg, T., Crapeau, M., Arriaga, A., O'Carroll, A., Coppens, D., Munro, R., and Calbet, X.: IASI on Metop-A: Operational Level 2 retrievals after five years in orbit, Journal of Quantitative Spectroscopy and Radiative Transfer, 113, 1340–1371, https://doi.org/10.1016/j.jqsrt.2012.02.028, 2012.

Borbas, E. E. and Ruston, B. C.: The RTTOV UWiremis IR land surface emissivity module, EUMETSAT, 2010.

Bouwman, L., Daniel, J. S., Davidson, E. A., de Klein, C., Holland, E., Ju, X., Kanter, D., Oenema, O., Ravishankara, A., Skiba, U. M., et al.: Drawing down N2O to protect climate and the ozone layer. A UNEP Synthesis Report, United Nations Environment Programme (UNEP), 2013.

Butterbach-Bahl, K., Baggs, E. M., Dannenmann, M., Kiese, R., and Zechmeister-Boltenstern, S.: Nitrous oxide emissions from soils: how well do we understand the processes and their controls?, Philosophical Transactions of the Royal Society of London B: Biological Sciences, 368, 20130 122, https://doi.org/10.1098/rstb.2013.0122, 2013.

Ciais, P., Sabine, C., Bala, G., Bopp, L., Brovkin, V., Canadell, J., Chhabra, A., DeFries, R., Galloway, J., Heimann, M., et al.: Carbon and other biogeochemical cycles, in: Climate change 2013: the physical science basis. Contribution of Working Group I to the Fifth Assessment Report of the Intergovernmental Panel on Climate Change, pp. 465–570, Cambridge University Press, 2014.

Clerbaux, C., Boynard, A., Clarisse, L., George, M., Hadji-Lazaro, J., Herbin, H., Hurtmans, D., Pommier, M., Razavi, A., Turquety, S., et al.: Monitoring of atmospheric composition using the thermal infrared IASI/MetOp sounder, Atmospheric Chemistry and Physics, 9, 6041–6054, https://doi.org/10.5194/acp-9-6041-2009, 2009.

Deeter, M. N., Edwards, D. P., Gille, J. C., and Drummond, J. R.: Sensitivity of MOPITT observations to carbon monoxide in the lower troposphere, Journal of Geophysical Research: Atmospheres, 112, n/a–n/a, https://doi.org/10.1029/2007JD008929, http://dx.doi.org/10.1029/2007JD008929, d24306, 2007.

Ganesan, A. L., Manning, A. J., Grant, A., Young, D., Oram, D. E., Sturges, W. T., Moncrieff, J. B., and O'Doherty, S.: Quantifying methane and nitrous oxide emissions from the UK and Ireland using a national-scale monitoring network, Atmospheric Chemistry and Physics, 15, 6393–6406, https://doi.org/10.5194/acp-15-6393-2015, http://www.atmos-chem-phys.net/15/6393/2015/, 2015.

García, O., Schneider, M., Hase, F., Blumenstock, T., Wiegele, A., Sepúlveda, E., and Gómez-Peláez, A.: Validation of the IASI operational CH4 and N2O products using ground-based Fourier Transform Spectrometer: preliminary results at the Izaña Observatory (28ºN, 17ºW), Annals of Geophysics, 56, https://doi.org/10.4401/ag-6326, 2014.

García, O. E., Sepúlveda, E., Schneider, M., Hase, F., August, T., Blumenstock, T., Kühl, S., Munro, R., Gómez-Peláez, A. J., Hultberg, T., et al.: Consistency and quality assessment of the Metop-A/IASI and Metop-B/IASI operational trace gas products (O3, CO, N2O, CH4, and CO2) in the subtropical North Atlantic, Atmospheric Measurement Techniques, 9, 2315–2333, https://doi.org/10.5194/amt-9-2315-2016, 2016.

Grieco, G., Masiello, G., Matricardi, M., and Serio, C.: Partially scanned interferogram methodology applied to IASI for the retrieval of CO, CO2, CH4 and N2O, Optics express, 21, 24 753–24 769, https://doi.org/10.1364/OE.21.024753, 2013.

Hilton, F., Armante, R., August, T., Barnet, C., Bouchard, A., Camy-Peyret, C., Capelle, V., Clarisse, L., Clerbaux, C., Coheur, P.-F., et al.: Hyperspectral Earth observation from IASI: Five years of accomplishments, Bulletin of the American Meteorological Society, 93, 347–370, https://doi.org/10.1175/BAMS-D-11-00027.1, 2012.

Hocking, J., Rayer, P., Rundle, D., Saunders, R., Matricardi, M., Geer, A., Brunel, P., and Vidot, J.: RTTOV v11 Users Guide, NWP SAF, 2015.

Inness, A., Baier, F., Benedetti, A., Bouarar, I., Chabrillat, S., Clark, H., Clerbaux, C., Coheur, P., Engelen, R. J., Errera, Q., Flemming, J., George, M., Granier, C., Hadji-Lazaro, J., Huijnen, V., Hurtmans, D., Jones, L., Kaiser, J. W., Kapsomenakis, J., Lefever, K., Leitão, J., Razinger, M., Richter, A., Schultz, M. G., Simmons, A. J., Suttie, M., Stein, O., Thépaut, J.-N., Thouret, V., Vrekoussis, M., Zerefos, C., and the MACC team: The MACC reanalysis: an 8 yr data set of atmospheric composition, Atmospheric Chemistry and Physics, 13, 4073–4109, https://doi.org/10.5194/acp-13-4073-2013, http://www.atmos-chem-phys.net/13/4073/2013/, 2013.

Kangah, Y., Ricaud, P., Attié, J.-L., Saitoh, N., Hauglustaine, D. A., Wang, R., El Amraoui, L., Zbinden, R., and Delon, C.: Summertime upper tropospheric nitrous oxide over the Mediterranean as a footprint of Asian emissions, Journal of Geophysical Research: Atmospheres, 122, 4746–4759, https://doi.org/10.1002/2016JD026119, http://dx.doi.org/10.1002/2016JD026119, 2016JD026119, 2017.

Kort, E., Patra, P., Ishijima, K., Daube, B., Jimenez, R., Elkins, J., Hurst, D., Moore, F., Sweeney, C., and Wofsy, S.: Tropospheric distribution and variability of N2O: Evidence for strong tropical emissions, Geophysical Research Letters, 38, https://doi.org/10.1029/2011GL047612, 2011.

Matricardi, M.: Technical Note: An assessment of the accuracy of the RTTOV fast radiative transfer model using IASI data, Atmos. Chem. Phys, 9, 6899–6913, https://doi.org/10.5194/acp-9-6899-2009, 2009.

Pougatchev, N., August, T., Calbet, X., Hultberg, T., Oduleye, O., Schlüssel, P., Stiller, B., Germain, K. S., and Bingham, G.: IASI temperature and water vapor retrievals–error assessment and validation, Atmospheric Chemistry and Physics, 9, 6453–6458, https://doi.org/10.5194/acp-9-6453-2009, 2009.

Ravishankara, A., Daniel, J. S., and Portmann, R. W.: Nitrous oxide (N2O): the dominant ozone-depleting substance emitted in the 21st century, science, 326, 123–125, https://doi.org/10.1126/science.1176985, 2009.

Ricaud, P., Attié, J.-L., Teyssedre, H., Amraoui, L. E., Peuch, V.-H., Matricardi, M., and Schluessel, P.: Equatorial total column of nitrous oxide as measured by IASI on MetOp-A: implications for transport processes, Atmospheric Chemistry and Physics, 9, 3947–3956, https://doi.org/10.5194/acp-9-3947-2009, 2009a.

Ricaud, P., Pommereau, J.-P., Attié, J.-L., Flochmoën, E. L., Amraoui, L. E., Teyssedre, H., Peuch, V.-H., Feng, W., and Chipperfield, M.: Equatorial transport as diagnosed from nitrous oxide variability, Atmospheric Chemistry and Physics, 9, 8173–8188, https://doi.org/10.5194/acpd-9-4899-2009, 2009b.

Rodgers, C. D. et al.: Inverse methods for atmospheric sounding: theory and practice, vol. 2, World scientific Singapore, 2000.

Saunders, R., Matricardi, M., and Brunel, P.: A fast radiative transfer model for assimilation of satellite radiance observations-RTTOV-5, European Centre for Medium-Range Weather Forecasts, 1999.

Sawa, Y., Machida, T., Matsueda, H., Niwa, Y., Tsuboi, K., Murayama, S., Morimoto, S., and Aoki, S.: Seasonal changes of CO2, CH4, N2O, and SF6 in the upper troposphere/lower stratosphere over the Eurasian continent observed by commercial airliner, Geophysical Research Letters, 42, 2001–2008, https://doi.org/10.1002/2014GL062734, 2015.

Seemann, S. W., Borbas, E. E., Knuteson, R. O., Stephenson, G. R., and Huang, H.-L.: Development of a global infrared land surface emissivity database for application to clear sky sounding retrievals from multispectral satellite radiance measurements, Journal of Applied Meteorology and Climatology, 47, 108–123, https://doi.org/10.1175/2007JAMC1590.1, 2008.

Sherlock, V. and Saunders, R.: ISEM-6: Infrared surface emissivity model for RTTOV-6, NWP-SAF report, 1999.

Stein, A., Draxler, R. R., Rolph, G. D., Stunder, B. J., Cohen, M., and Ngan, F.: NOAA's HYSPLIT atmospheric transport and dispersion modeling system, Bulletin of the American Meteorological Society, 96, 2059–2077, https://doi.org/10.1175/BAMS-D-14-00110.1, 2015.

Syakila, A. and Kroeze, C.: The global nitrous oxide budget revisited, Greenhouse Gas Measurement and Management, 1, 17–26, https://doi.org/10.3763/ghgmm.2010.0007, 2011.

Turquety, S., Hadji-Lazaro, J., Clerbaux, C., Hauglustaine, D., Clough, S., Cassé, V., Schlüssel, P., and Mégie, G.: Operational trace gas retrieval algorithm for the Infrared Atmospheric Sounding Interferometer, Journal of Geophysical Research: Atmospheres, 109, https://doi.org/10.1029/2004JD004821, 2004.

Wofsy, S. et al.: HIPPO Merged 10-Second Meteorology and Atmospheric Chemistry and Aerosol Data (R_20121129), Carbon Dioxide Information Analysis Center, Oak Ridge National Laboratory and Oak Ridge and Tennessee.[Avaialble at http://dx. doi. org/10.3334/CDIAC/hippo_010,(Release 20121, 129)], 2012.

Wofsy, S. C.: HIAPER Pole-to-Pole Observations (HIPPO): fine-grained, global-scale measurements of climatically important atmospheric gases and aerosols, Philosophical Transactions of the Royal Society of London A: Mathematical, Physical and Engineering Sciences, 369, 2073–2086, https://doi.org/10.1098/rsta.2010.0313, 2011.

Xiong, X., Barnet, C., Maddy, E., Gambacorta, A., King, T., and Wofsy, S.: Mid-upper tropospheric methane retrieval from IASI and its validation, Atmospheric Measurement Techniques, 6, 2255, https://doi.org/10.5194/amt-6-2255-2013, 2013.

Xiong, X., Maddy, E. S., Barnet, C., Gambacorta, A., Patra, P. K., Sun, F., and Goldberg, M.: Retrieval of nitrous oxide from Atmospheric Infrared Sounder: Characterization and validation, Journal of Geophysical Research: Atmospheres, 119, 9107–9122, https://doi.org/10.1002/2013JD021406, 2014.

Atmos. Meas. Tech. Discuss., https://doi.org/10.5194/amt-2018-21
Manuscript under review for journal Atmos. Meas. Tech.
Discussion started: 13 April 2018

Atmospheric Measurement Techniques Discussions

Parameters	σ_a **in B1**	σ_a **in B2**
N_2O	4 %	4 %
H_2O	30 %	10 %
Temperature	1 K	1 K
CH_4	2 %	not retrieved
CO	not retrieved	10 %
CO_2	not retrieved	2 %
Surface temperature	2 K	2 K
Surface emissivity	10 %	10 %

Table 1. A priori standard deviation errors (σ_a) used for each retrieved parameter in B1 and B2.

Atmos. Meas. Tech. Discuss., https://doi.org/10.5194/amt-2018-21
Manuscript under review for journal Atmos. Meas. Tech.
Discussion started: 13 April 2018

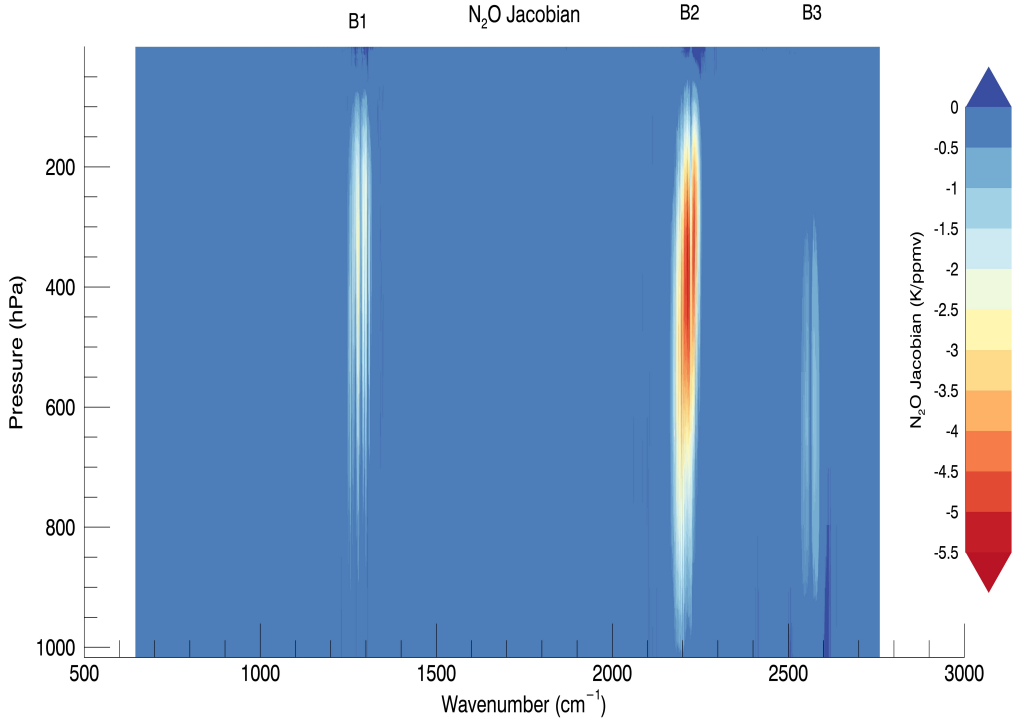

Figure 1. N_2O Jacobian in brightness temperature calculated by RTTOV over IASI spectral range and for an atmospheric situation at 142.96°W and 11.76°N.

Atmos. Meas. Tech. Discuss., https://doi.org/10.5194/amt-2018-21
Manuscript under review for journal Atmos. Meas. Tech.
Discussion started: 13 April 2018

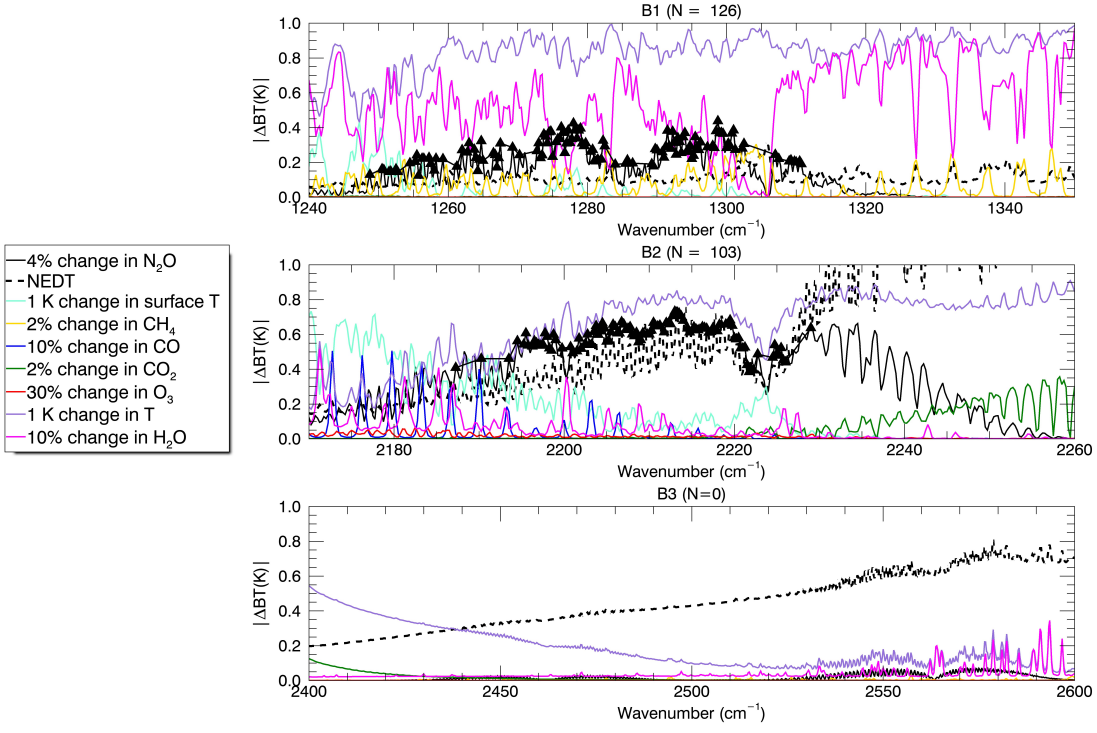

Figure 2. Absolute change of brightness temperature ($|\Delta BT|$) for 4% change in N_2O (black solid line), 10% change in H_2O (pink), 2% change in CH_4 (yellow), 10% change in CO (blue), 2% change in CO_2 (dark green), 30% change in O_3 (red), 1K change in temperature (purple) and surface temperature (light green), for the bands B1 (top), B2 (middle), B3 (bottom) at 142.96°W and 11.76°N. The black triangles mark the channels selected for the retrievals. The dashed black line represents the Noise Equivalent Delta Temperature (NEDT) of IASI level 1c measurements.

Atmos. Meas. Tech. Discuss., https://doi.org/10.5194/amt-2018-21
Manuscript under review for journal Atmos. Meas. Tech.
Discussion started: 13 April 2018

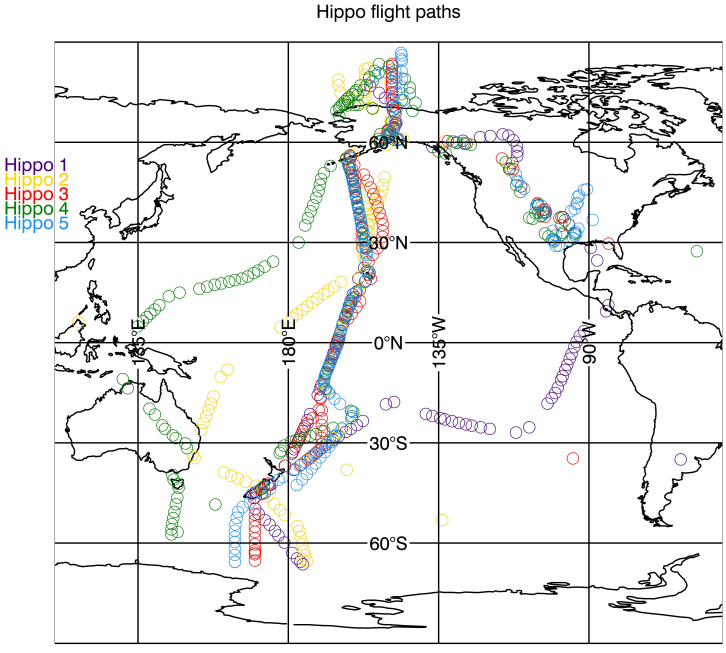

Figure 3. Flight paths of HIPPO campaigns used for GOSAT N_2O validation: HIPPO 1 (January 2009, purple), HIPPO 2 (October-November 2009, yellow), HIPPO 3 (March-April 2010,red), HIPPO 4 (June-July 2011, green) and HIPPO 5 (August-September 2011, blue).

Atmos. Meas. Tech. Discuss., https://doi.org/10.5194/amt-2018-21
Manuscript under review for journal Atmos. Meas. Tech.
Discussion started: 13 April 2018

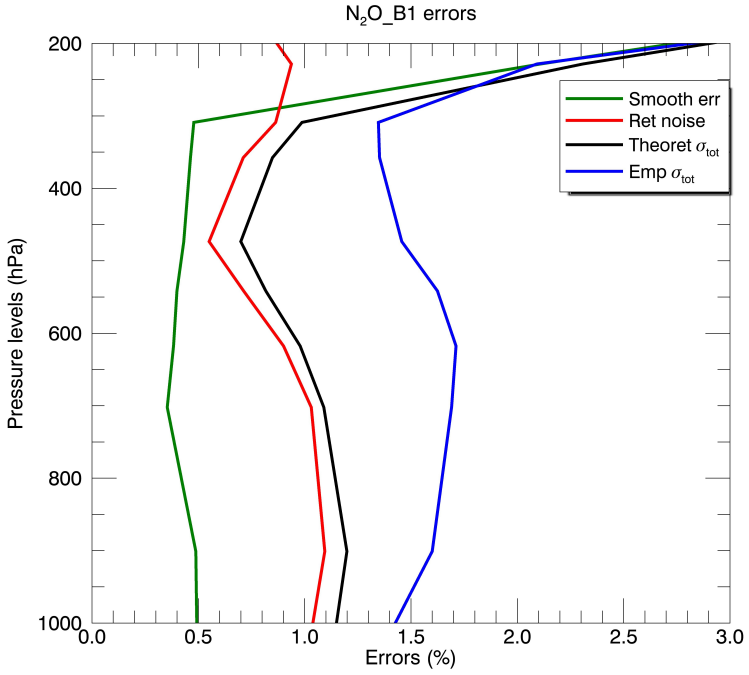

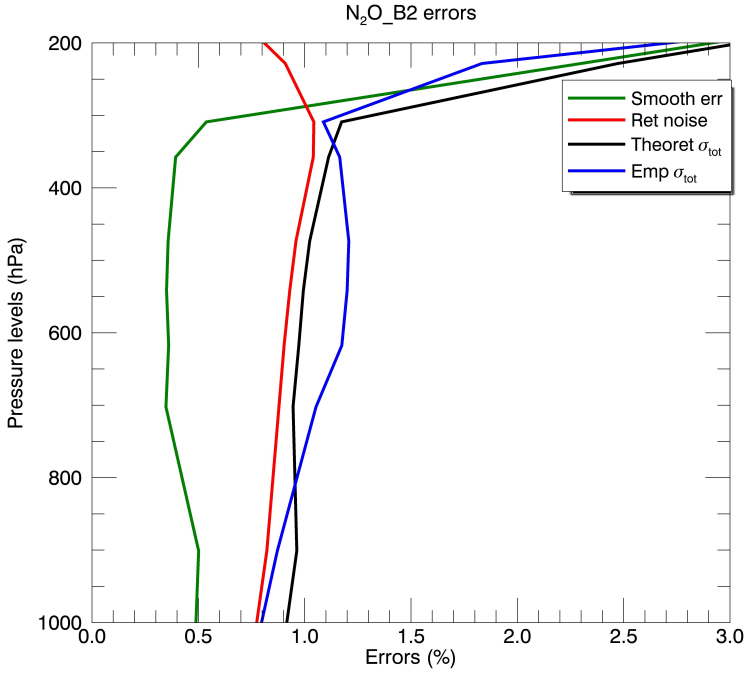

Figure 4. Top: Standard deviations of the smoothing errors (solid green line), the retrieval noise (solid red line), the theoretical total errors (solid blue line) and the empirical total errors (solid black line) on N_2O_B1 averaged over a set of 26850 retrievals along the HIPPO campaigns flight paths. Bottom: same as top but for N_2O_B2.

Atmos. Meas. Tech. Discuss., https://doi.org/10.5194/amt-2018-21
Manuscript under review for journal Atmos. Meas. Tech.
Discussion started: 13 April 2018

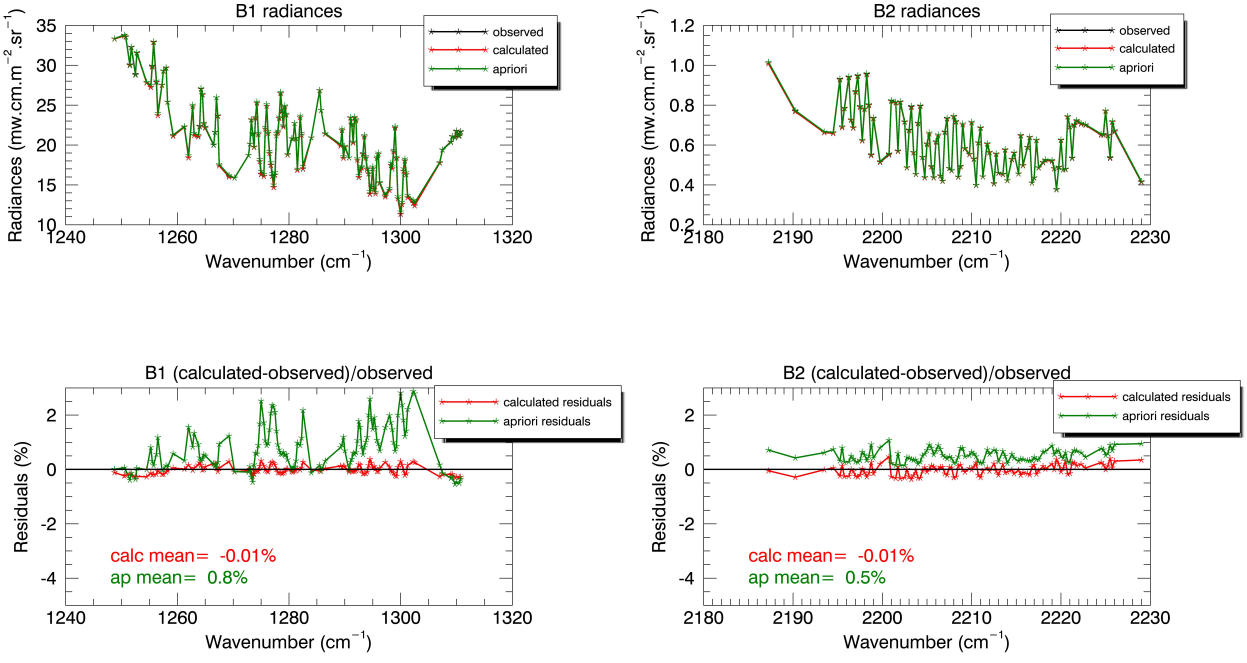

Figure 5. Top: Averaged level 1c observed radiances (black) and calculated radiances using a priori (green) and using retrievals (red) for the bands B1 (left) and B2 (right). Bottom: a priori (green) and calculated (red) residuals ((calc−obs)/obs) for the bands B1 (left) and B2 (right)).

Atmos. Meas. Tech. Discuss., https://doi.org/10.5194/amt-2018-21
Manuscript under review for journal Atmos. Meas. Tech.
Discussion started: 13 April 2018

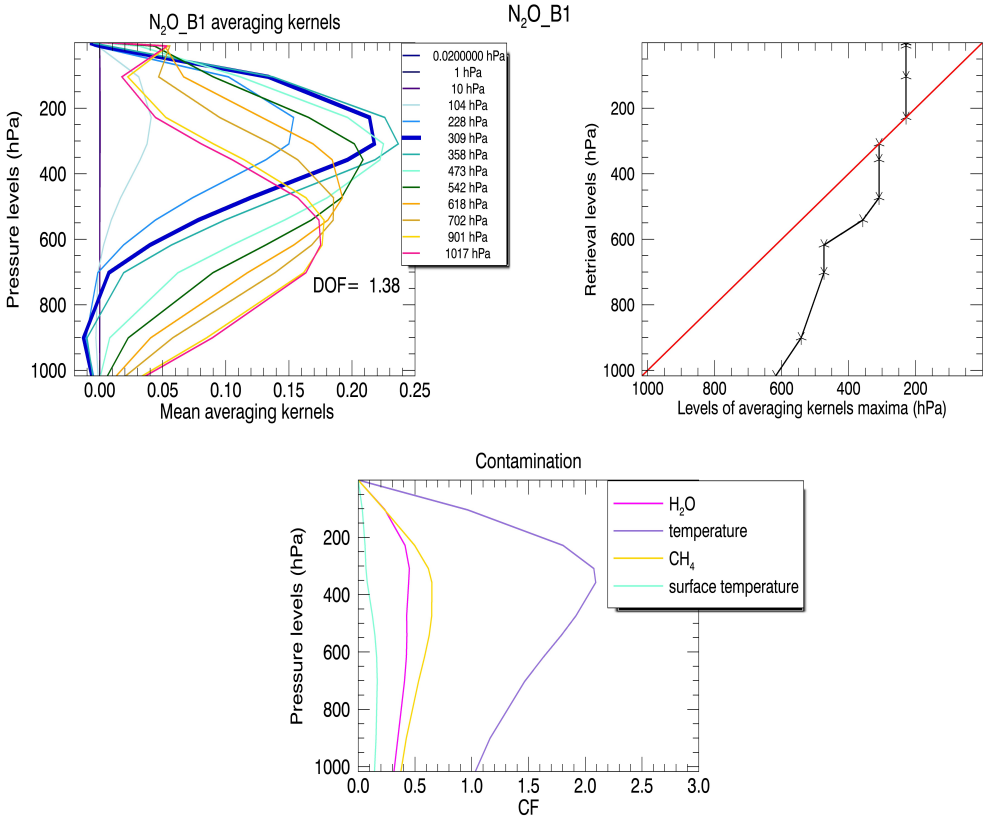

Figure 6. Top-left: Normalized averaging kernels averaged for all the N_2O_B1 over the HIPPO campaigns flight paths (26850 pixels).Top-right: levels of the averaging kernels maximum. Bottom: Mean surface temperature (green), CH_4 (yellow), temperature (purple) and H_2O (pink) CF on N_2O_B1.

Atmos. Meas. Tech. Discuss., https://doi.org/10.5194/amt-2018-21
Manuscript under review for journal Atmos. Meas. Tech.
Discussion started: 13 April 2018

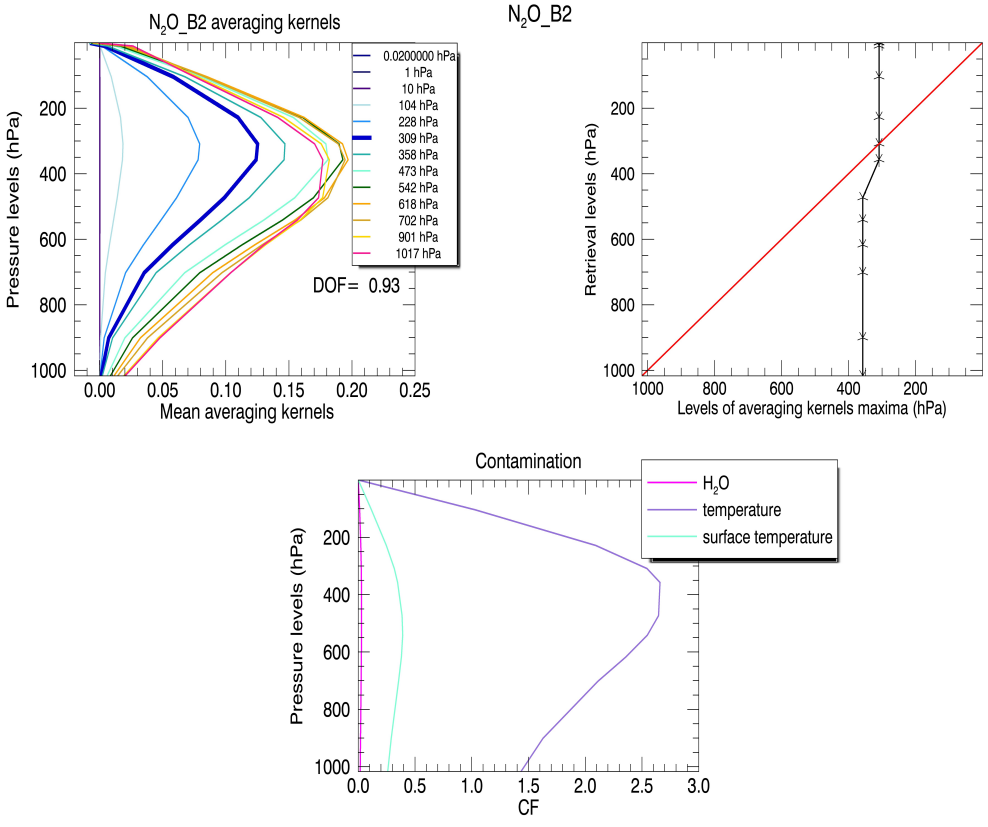

Figure 7. Same as Figure 6 for N_2O_B2.

Atmos. Meas. Tech. Discuss., https://doi.org/10.5194/amt-2018-21
Manuscript under review for journal Atmos. Meas. Tech.
Discussion started: 13 April 2018

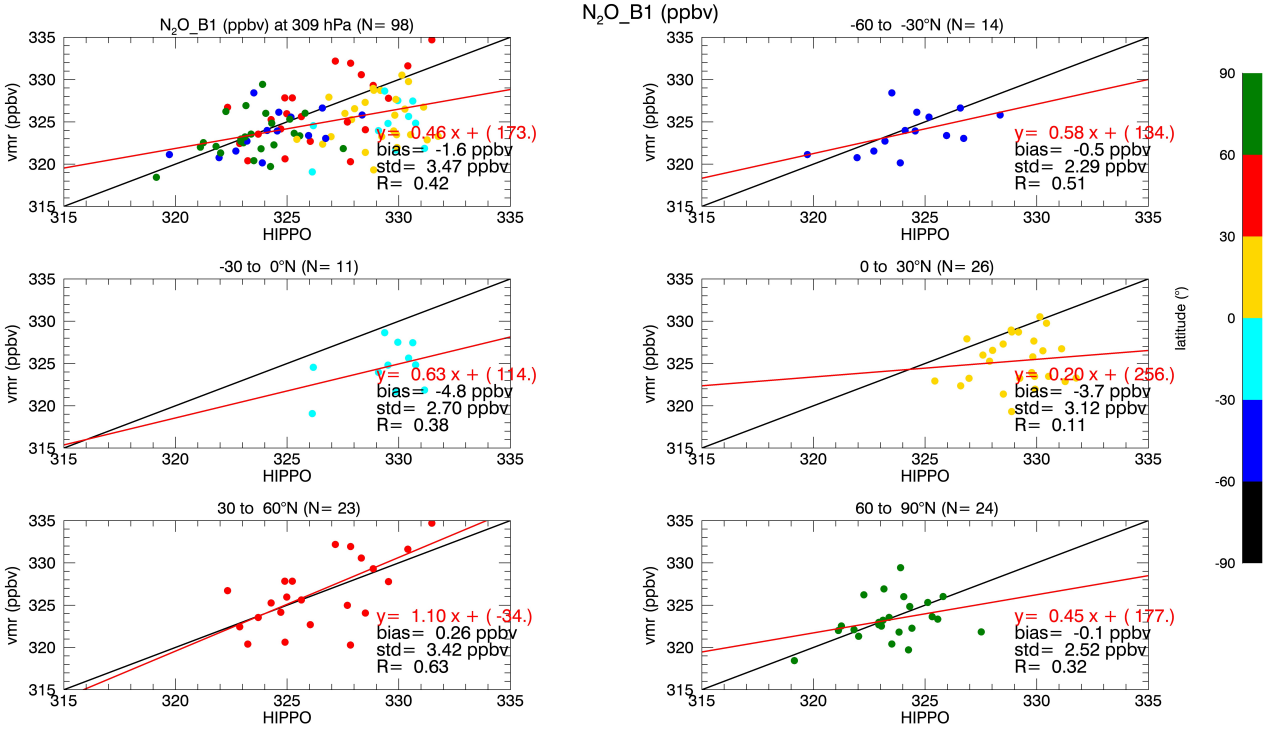

Figure 8. HIPPO N_2O measurements vs N_2O_B1 at 309 hPa averaged within a box of ± 200 km and a temporal window of ± 12h around the HIPPO measurements. The black and red lines represent the first bisector (y=x) and the linear regression line, respectively. The colorbar represents the different latitude bands of the HIPPO measurements. N is the number of collocated pixels.

Atmos. Meas. Tech. Discuss., https://doi.org/10.5194/amt-2018-21
Manuscript under review for journal Atmos. Meas. Tech.
Discussion started: 13 April 2018

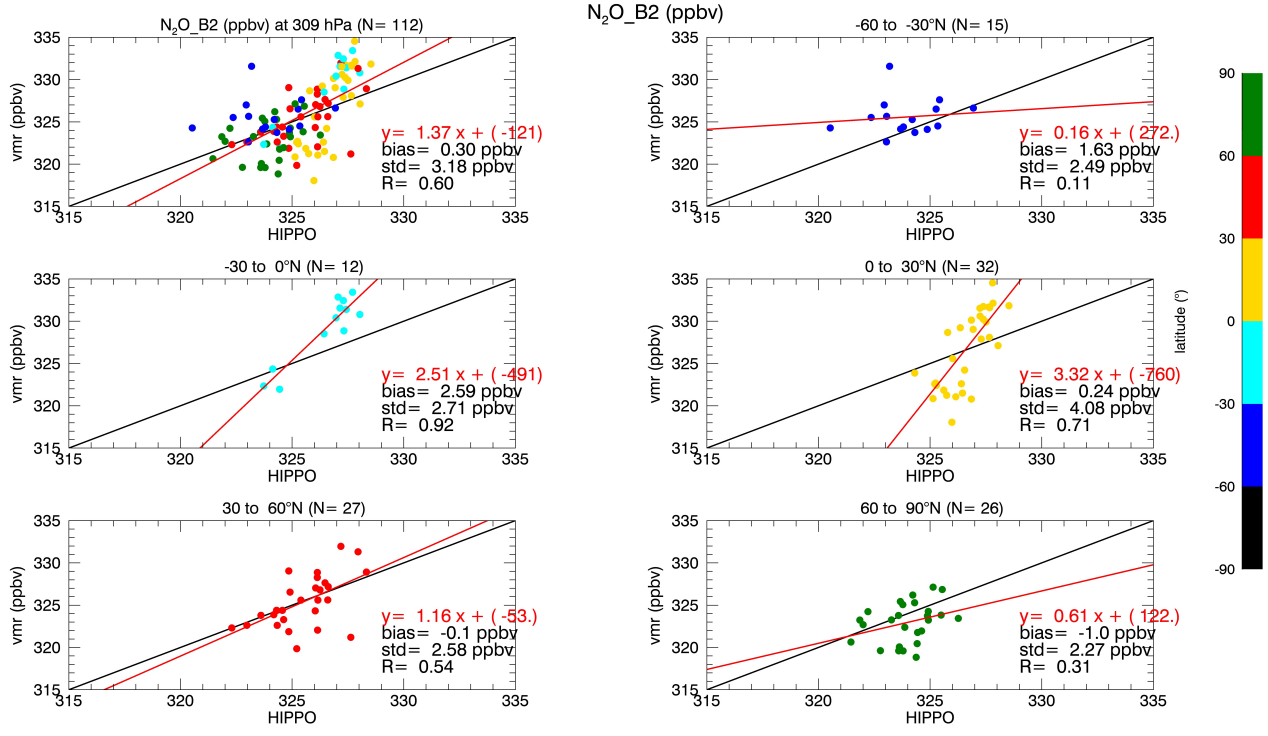

Figure 9. Same as Figure 8 but for the N_2O_B2.

Atmos. Meas. Tech. Discuss., https://doi.org/10.5194/amt-2018-21
Manuscript under review for journal Atmos. Meas. Tech.
Discussion started: 13 April 2018

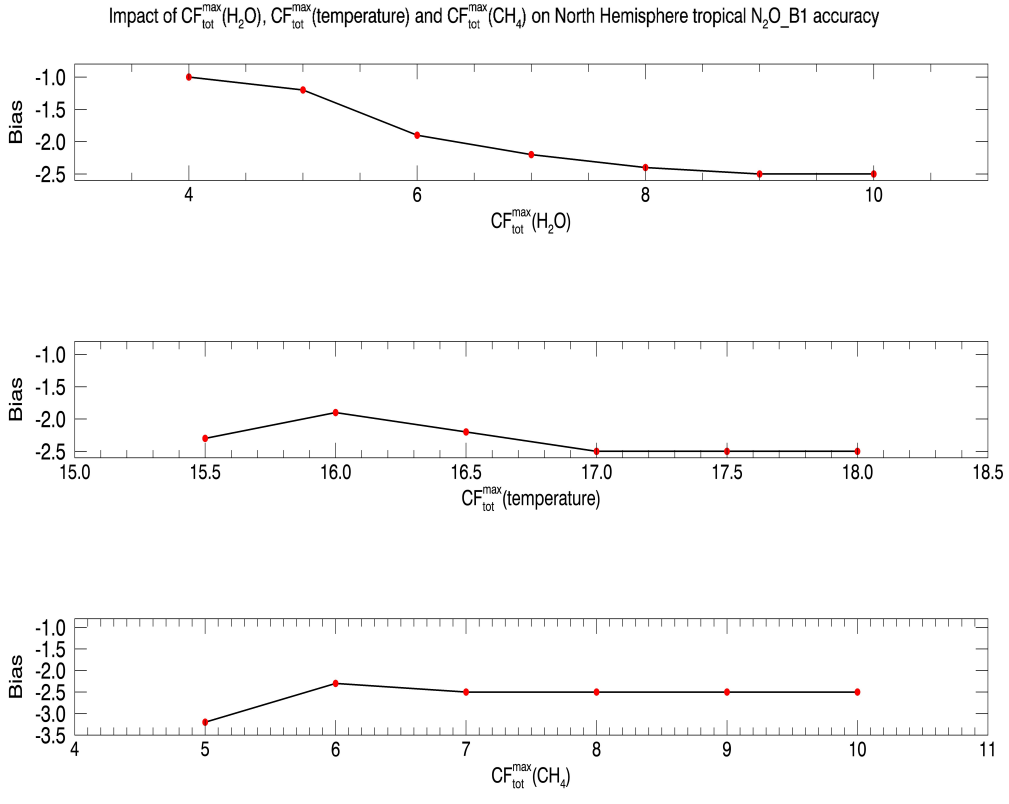

Figure 10. Mean bias corresponding to N_2O_B1-HIPPO collocated pixels in the northern hemisphere tropical regions (0-30°N) for different values of CF_{tot}^{max}(H_2O) (top), CF_{tot}^{max}(temperature) (middle) and CF_{tot}^{max}(CH_4) (bottom) .

Atmos. Meas. Tech. Discuss., https://doi.org/10.5194/amt-2018-21
Manuscript under review for journal Atmos. Meas. Tech.
Discussion started: 13 April 2018

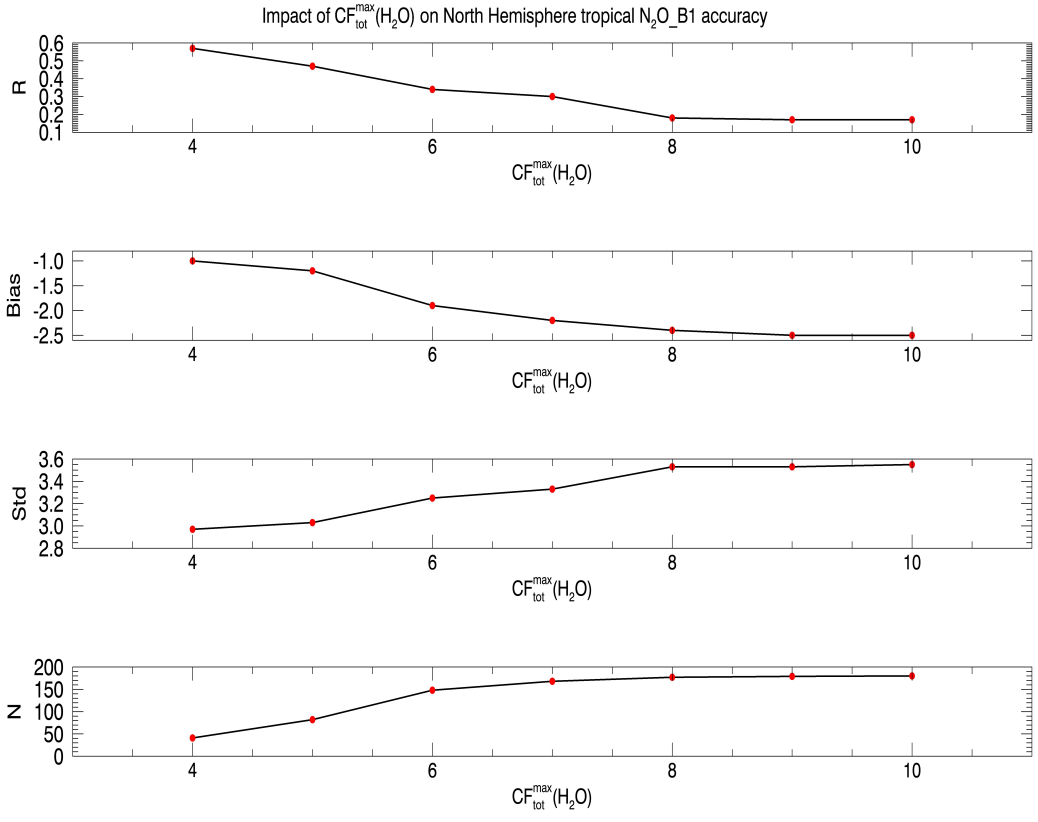

Figure 11. From top to bottom: Pearson linear correlation coefficient (R), mean bias, std error and number of IASI retrieved pixels (N) for different values of CF_{tot}^{max}(H$_2$O) corresponding to N$_2$O_B1-HIPPO collocated pixels in the northern hemisphere tropical regions (0-30°N)

.

Atmos. Meas. Tech. Discuss., https://doi.org/10.5194/amt-2018-21
Manuscript under review for journal Atmos. Meas. Tech.
Discussion started: 13 April 2018

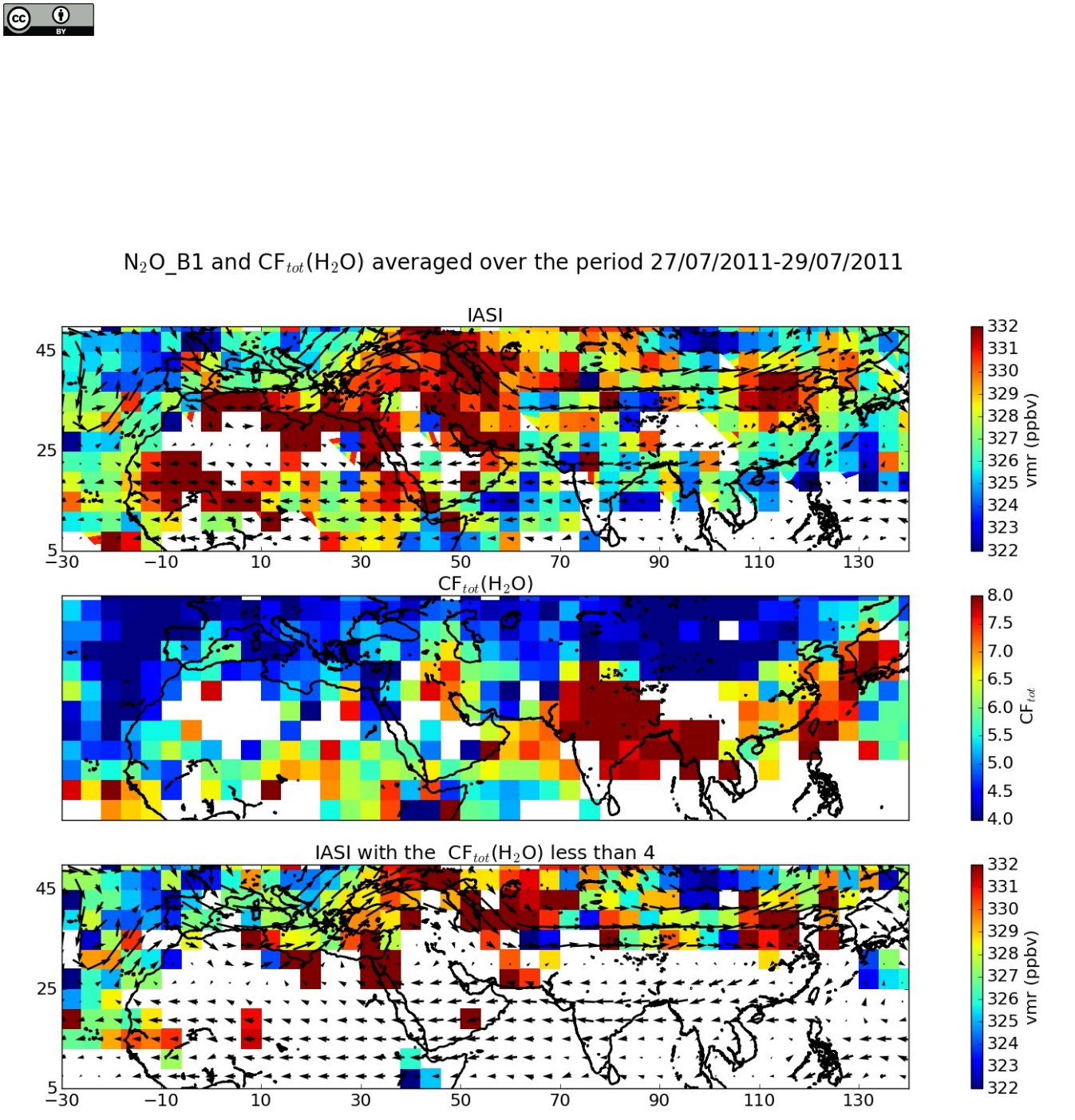

Figure 12. N_2O_B1 (top), $CF_{tot}(H_2O)$ (middle) and N_2O_B1 filtered with $CF_{tot}^{max}(H_2O)$ equal to 4 (bottom) averaged over the period 27-29 July 2011. Horizontal winds from ERA-Interim reanalysis at 300 hPa are superimposed to N_2O_B1.

Atmos. Meas. Tech. Discuss., https://doi.org/10.5194/amt-2018-21
Manuscript under review for journal Atmos. Meas. Tech.
Discussion started: 13 April 2018

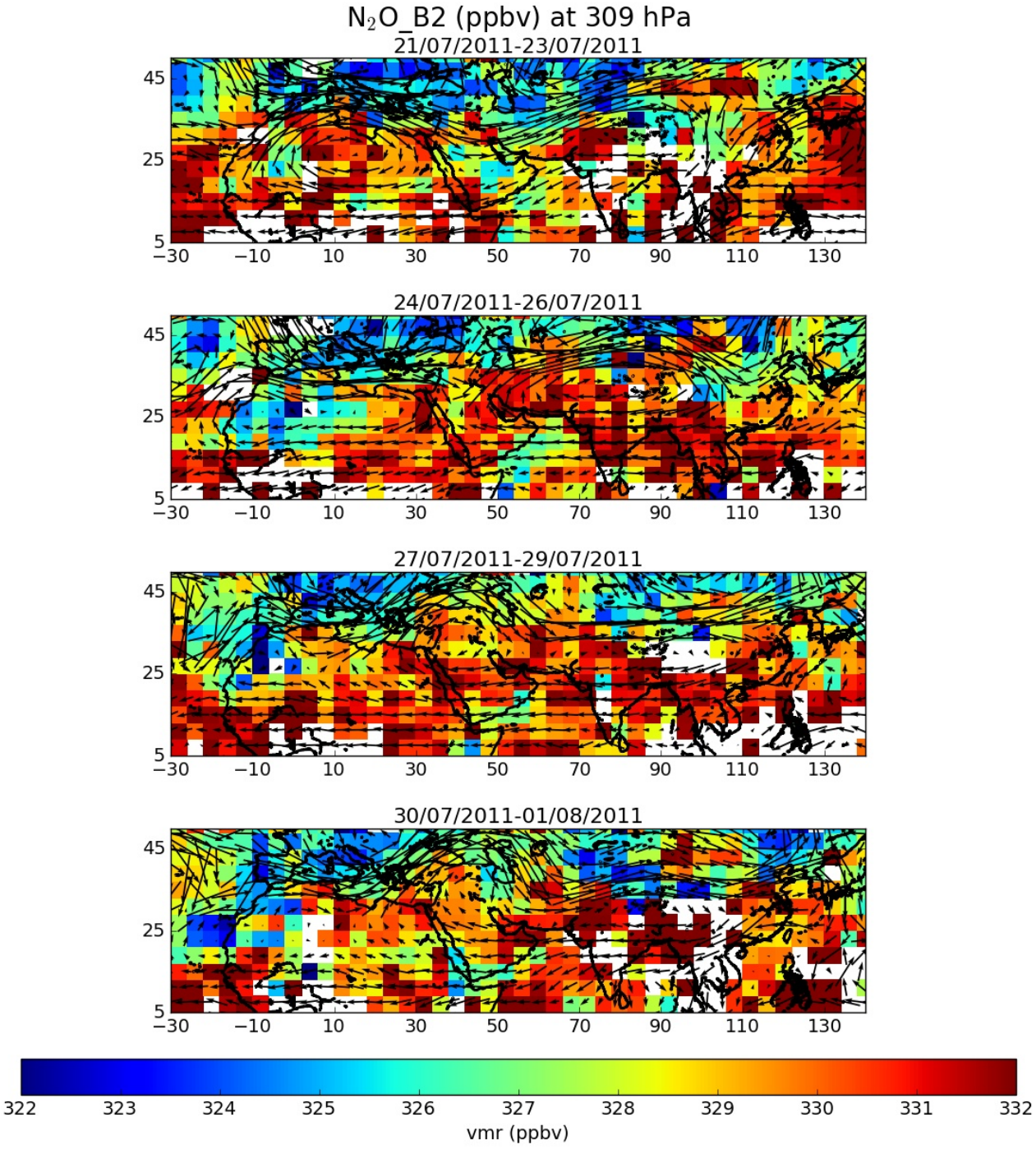

Figure 13. N_2O_B2 at 309 hPa and horizontal winds from ERA-Interim reanalysis at 300 hPa averaged over the periods (from top to bottom) 21-23 July, 24-26 July, 27-29 July and 30 July-01 August 2011.

Atmos. Meas. Tech. Discuss., https://doi.org/10.5194/amt-2018-21
Manuscript under review for journal Atmos. Meas. Tech.
Discussion started: 13 April 2018

Atmospheric Measurement Techniques Discussions

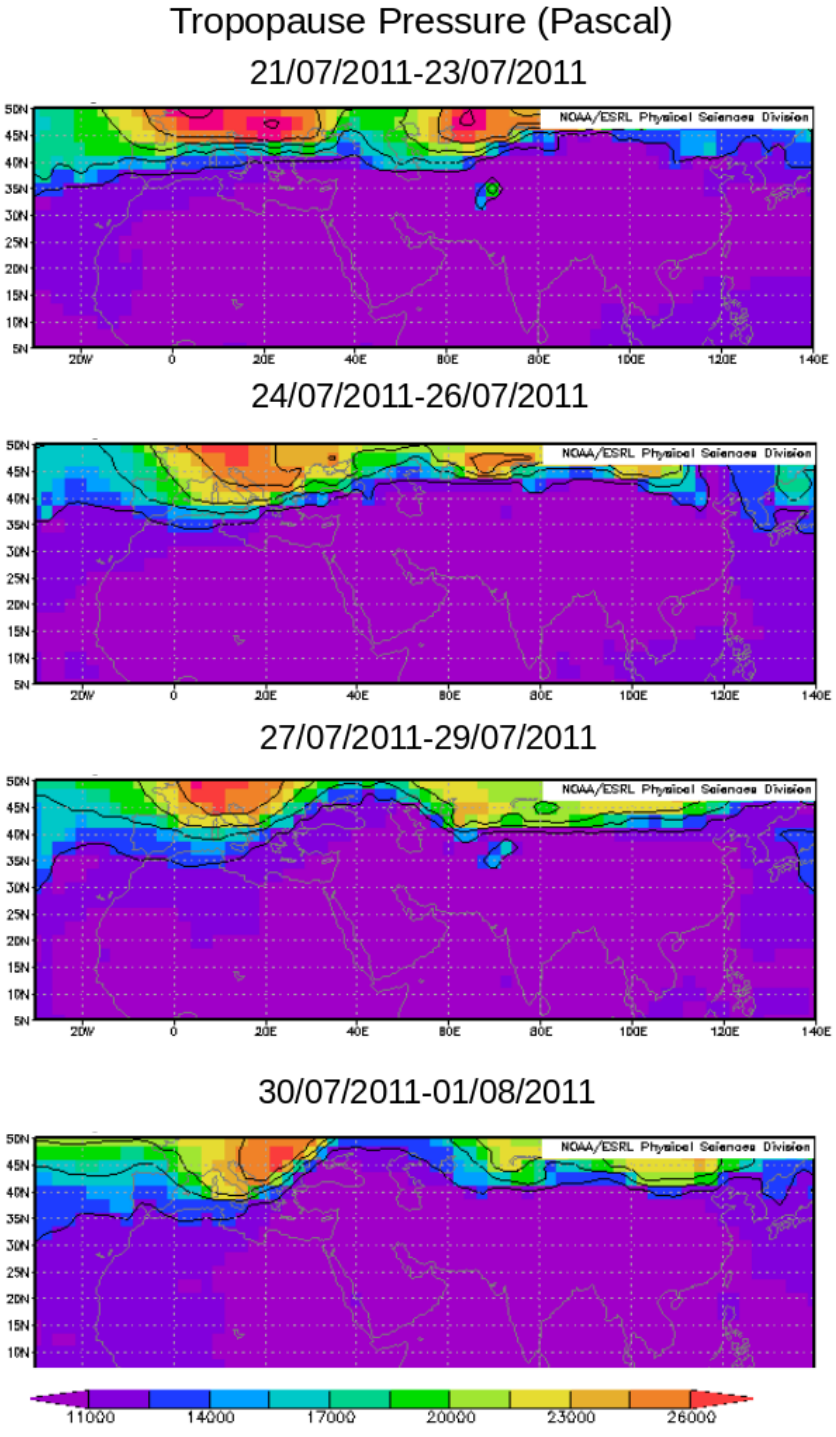

Figure 14. Tropopause pressure levels from the NCEP/NCAR 40-year reanalysis averaged over the periods (from top to bottom) 21-23 July, 24-26 July, 27-29 July and 30 July-01 August 2011.

Atmos. Meas. Tech. Discuss., https://doi.org/10.5194/amt-2018-21
Manuscript under review for journal Atmos. Meas. Tech.
Discussion started: 13 April 2018

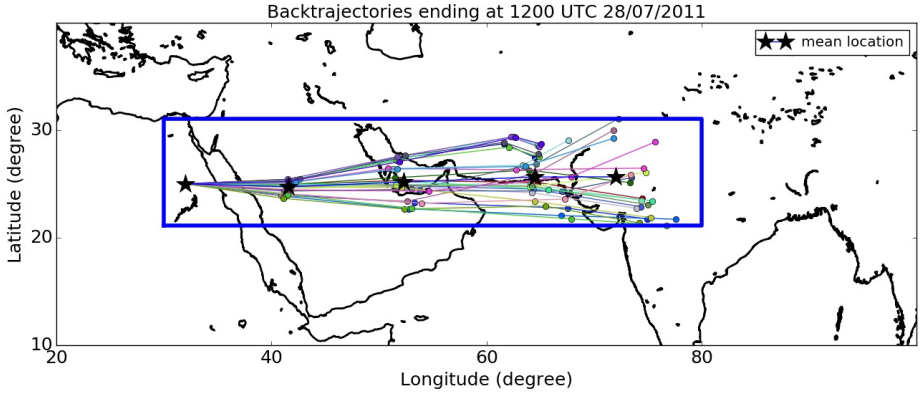

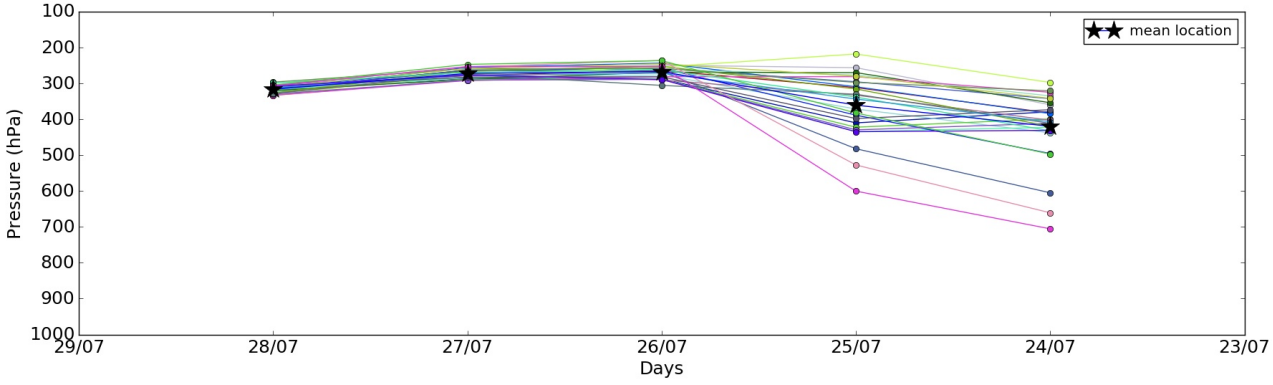

Figure 15. Top: Spatial evolution of a backtrajectory ensemble calculation performed with the HYSPLIT model and ending on 28 July 2011 at 12h00 UTC. Each member is calculated by offsetting a central point at 25°N, 32°E and 9100 m of altitude (∼306 hPa). The offset is 0.5 degree in the horizontal and 1 sigma unit in the vertical. The black stars represent the mean trajectory and the blue box which represents the latitude range of the trajectories is used to calculate an Hovmöller diagram along the longitudinal path of the air mass (see Figure 16). Bottom: The same backtrajectories presented above but as a function of pressure and time.

Atmos. Meas. Tech. Discuss., https://doi.org/10.5194/amt-2018-21
Manuscript under review for journal Atmos. Meas. Tech.
Discussion started: 13 April 2018

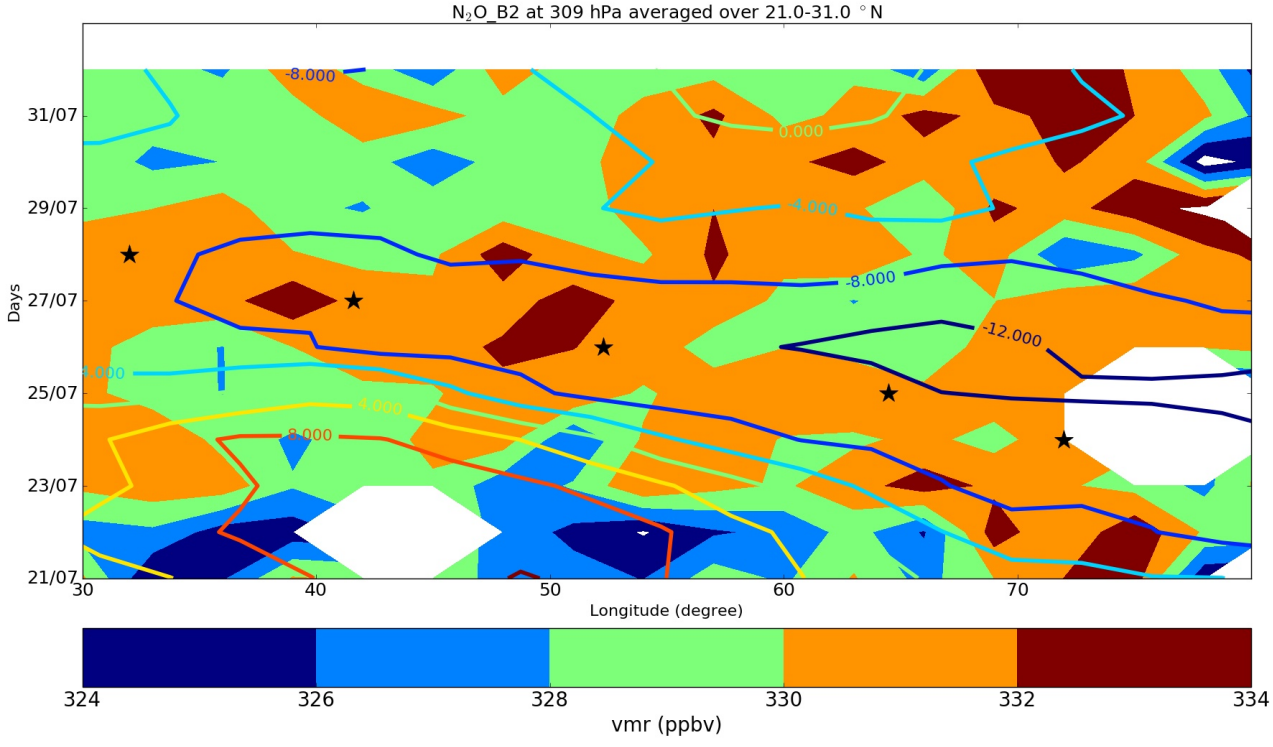

Figure 16. Hovmöller diagram showing N_2O_B2 at 309 hPa superimposed with zonal winds from ERA-Interim at 300 hPa (solid line contour) calculated by averaging the retrievals over the latitude range 21-31 °N (blue rectangle from figure 15) and on a daily basis. The black stars represent the mean trajectory of the backtrajectory ensemble (see Figure 15).

Code and data availability. The presented IASI N_2O retrievals (for the months June and July 2011 and over the spatial domain studied in this paper) are available by request to the author. A database with global N_2O retrievals on a daily basis is currently in preparation. The HIPPO data can be freely downloaded at http://hippo.ucar.edu/. IASI L1C and L2 data are available at the EUMETSAT Data Centre (www.eumetsat.int.). The MIPAS reference atmosphere profiles can be downloaded from http://www.atm.ox.ac.uk/RFM/atm/. The RTTOV software can be downloaded at https://www.nwpsaf.eu/site/software/rttov/download/ after registration.

Acknowledgements. We would like to thank the following institutes and programs for funding our study: Centre National de la Recherche Scientifique-Institut National des Sciences de l'Univers (CNRS-INSU), Centre National des Etudes Spatiales (CNES), Agence de l'Environnement et de la Maîtrise de l'Energie (ADEME) through the program the Mediterranean Integrated Studies at Regional And Local Scales (MISTRALS), Chemistry-Aerosol Mediterranean Experiment (ChArMEx), Météo-France, and Airbus Defense and Space for funding Y. Kangah's PhD thesis. We would like to thank also the NOAA/OAR/ESRL PSD, Boulder, Colorado, USA, for provided the NCEP Reanalysis data via their Web site at http://www.esrl.noaa.gov/psd/.